

Study on refined mathematical model of solar chimney power plant integrated with seawater desalination and the influence of dewing

Lu Zuo[*, a], Long Huang [a], Pengzhan Dai [a], Yu Chen [a], Shi Chen [a], Yunting Ge [b]
[a] College of Energy and Electrical Engineering, Hohai University, Nanjing, China
[b] School of the Built Environment and Architecture, London South Bank University, London, UK

Abstract: In order to more accurately evaluate the operation and output characteristics of the solar chimney power plant integrated seawater desalination, a refined mathematical model for unsteady heat and mass transfer was built under consideration of the convection heat transfer mechanism of the collector, dewing phenomenon, and the disturbance to the hot airflow caused by the oblique-toothed flow channel boundary. The influence of nighttime dewing and humid environments on system performance was discussed. The results show that it is feasible and more appropriate to use the forced convection heat transfer coefficient of bellows to consider the influence of the oblique-toothed flow channel boundary; the refined mathematical model is also more accurate and reliable. Due to the effect of seawater heat storage, dewing has little effect on system performance, and the integrated system has a better anti-dewing negative impact characteristic. However, when the ambient humidity reached a higher level, dewing had a greater negative impact on freshwater production. The critical value of relative humidity for dewing to occur is 51%. When the relative humidity increases from 45% to 60%, the daily utilization efficiency of solar energy decreases from 27.4% to 22.5%.

Keywords: solar chimney power plant; seawater desalination; dewing phenomenon; convection heat transfer; refined model

1 Introduction

The shortage of energy and freshwater resources are two problems facing the

[*] Corresponding author.
E-mail address: zuoluhhu@163.com (L. Zuo).

world. Solar energy has become one of the important choices for people to deal with energy shortage, climate change, and energy conservation and emission reduction due to its advantages of cleanness, environmental protection, sustainability, and long-term. It has become a common trend for countries all over the world to develop the cause of seawater desalination and ask for freshwater from the sea. Using solar energy to desalinate seawater and establishing solar power system respectively solved the above problems from two aspects to a certain extent. The solar chimney power system with integration of seawater desalination combining solar chimney power technology, solar energy heat storage technology, and solar evaporation condensation desalination seawater technology came into being.

Zuo et al.[1] set up a closed disc seawater distillation pool under the collector of the solar chimney power plant (SCPP), and proposed a solar chimney power plant integrated seawater desalination (SCPPSD) system. The integrated system inherits the power generation principle of the independent solar chimney power system, uses the disc distillation principle to produce freshwater, uses seawater to store heat, and realizes water-electricity cogeneration. Compared with the independent solar chimney power system, the integrated system not only has the original advantages, such as simple structure, convenient material collection, low construction and operation costs, and no harmful waste but also has high solar energy utilization efficiency and high comprehensive land utilization rate; Stable power generation day and night, improved power quality; In addition to producing electricity and freshwater, it can also make use of the evaporation and concentration of seawater to produce raw salt, with remarkable economic benefits. To strengthen the efficiency of SCPPSD, Zuo et al. proposed a series of SCPPSD expended systems by integrating unpowered wind supercharger[2], flue gas waste heat[3], vortex engine[4] and solar membrane distillation technology[5] respectively.

The heat and mass transfer mathematical model of SCPPSD and its extended system is based on the heat and mass transfer model of independent SCPP and solar disk distiller. In 1982, the Schlaich team built the world's first large-scale solar chimney power plant in Manzanares, Spain[6]. As early as in the research of the Spanish prototype SCPP test, Haaf et al.[7, 8] gave the energy balance equation in the collector and the theoretical power output formula of the turbine, but did not explicitly describe the selection of the heat transfer coefficient in the heat transfer process.

Bernardes and Weinrebe[9] developed the unsteady heat balance mathematical model of the collector area of the SCPP based on the cavity between the two parallel plates. Among them, the convection heat transfer coefficient between the collector cover and the hot airflow, and between the ground and the hot airflow is calculated by the calculation formula of the plate convection heat transfer coefficient, and the influence of forced convection or natural convection is considered. The maximum error between the mathematical model and the Spanish prototype in power output is only 1.9%. Pretorius and Kröger[10] analyzed the influence of the selection of convection heat transfer coefficient on the performance calculation of SCPP, made a detailed distinction between the convection heat transfer coefficient from the collector cover to the ambient air, from the collector cover to the hot airflow, and from the ground to the hot airflow, improved the selection scheme of the convection heat transfer coefficient, and adopted the heat transfer coefficient formula considering mixed convection and forced convection. Bernardes et al.[11] compared the influence of Bernardes' convective heat transfer coefficient scheme[9] and Pretorius' convective heat transfer coefficient scheme[10] on estimating SCPP performance. It is found that the heat transfer coefficient from the collector cover and the ground to hot airflow calculated by Pretorius is larger, and the heat loss of the collector cover to the ambient air is smaller; In Bernardes' scheme, the heat transfer coefficient from the collector cover to the ambient air is small, which also leads to lower heat loss of the collector cover to the ambient air. Therefore, the temperature variation of hot airflow calculated by the two schemes is similar.

Li et al.[12] built a one-dimensional steady-state mathematical model of SCPP considering the temperature lapse rates inside and outside the chimney and the flow loss, in which the Pretorius' convection heat transfer scheme was used, and studied the influence of the radius of the collector and the height of the chimney on the power output. Xu et al.[13] established a compressible heat and mass transfer model of SCPP considering air humidity, refined the transient calculation formula of multiphase flow and heat transfer in the system, and analyzed the influence of humidity on the output characteristics of SCPP. Khidhir et al.[14] developed the physical model and heat transfer model of the SCPP which has a reflector assisted heating chimney base, proposed the method of installing an absorption plate in the transition section to absorb reflected light to heat the airflow to improve the system efficiency, and analyzed it in combination with the test. In the research, the mathematical model is further modified based on the test data, and the error with the test value can be reduced to a minimum of 7%.

Bouchair[15] modeled the nonlinear steady-state heat transfer of the solar chimney ventilation system for building ventilation and studied the influence of altitude on the chimney outlet temperature, mass flow, and heat transfer coefficient. The results show that the altitude affects the performance of the system indirectly only by affecting the ambient temperature. Dahire et al.[16] developed a one-dimensional steady-state heat transfer model for an inclined solar chimney ventilation system with water vapor as a participating medium and hot airflow in the collector as a part of radiation heat transfer, the effects of the inclination angle of the collector and the height of the inlet clearance on the air exchange capacity of the system were studied. Ming et al.[17] set up a mixed energy storage layer of water and sand to make the output of SCPP system smooth, established a heat transfer mathematical model of SCPP with an energy storage layer, in which the convection heat transfer scheme of Bernardes was used, and the influence of the depth, area, and position of the water layer on the output fluctuation of the system is studied.

At present, Pretorius and Kröger's convective heat transfer coefficient scheme has been widely used in developing energy transfer models for SCPP and its integrated systems. Zuo et al.[18] based on the cavity between the two parallel plates to develop a SCPPSD all-weather unsteady-state mathematical model, Pretorius and Kröger's convective heat transfer coefficient scheme is also used to calculate the convective heat transfer coefficient between the boundary of the airflow channel and the hot airflow under the collector cover. In the extended systems[2-5], which enhance the performance of SCPPSD, the same convective heat transfer coefficient schemes are used in the energy transfer models.

Kiwan et al.[19] proposed a solar chimney power system that integrates photovoltaic power generation and desalination, in which photovoltaic panels are immersed in an open desalination pool to lower the temperature of the panels and improve power generation efficiency. The steady mathematical model of heat and mass transfer of the integrated system is established, and Pretorius' convection heat transfer scheme is also used in the mathematical model. The research results show that the system can generate 45.35% more electricity than independent photovoltaic power generation, the utilization factor of the system is increased by 757% compared with the conventional SCPP, and the economic benefit is greatly improved. Rahbar and Riasi[20] have designed a photovoltaic and desalination based solar chimney power plant (PVDSCP) system, based on the conventional SCPP energy transfer model, a one-dimensional heat and mass transfer mathematical model of PVDSCP was developed and the system performance was evaluated. The relative convective heat transfer coefficient of the hot airflow in the collector in the model adopts the scheme proposed by Pasumarthi and Sherif[21].

Using software—Fluent, Rahdan et al.[22] carried out a transient simulation of a two-dimensional solar chimney power plant integrated desalination model, and the effects of the divergent chimney, collector cover inclination, and closed still cover inclination on the performance of the hybrid system were studied. Hassan[23] designed a combined adsorption refrigeration solar chimney power plant integrated system, through the heat-absorbing plate installed on the ground of the collector area to transfer heat to the adsorption bed, to achieve the cogeneration of cooling capacity and electricity. The feasibility of the system is analyzed by developing the mathematical model of energy transmission. Alkhalidi and Al-Jraba'ah[24] designed a novel solar chimney power plant integrated desalination which uses concentrated solar energy to evaporate seawater and micro-steam turbines to replace the air turbine. The steam generated by heating seawater through a reflector drives a micro-steam turbine to generate electricity, and the work-done steam is condensed and collected in the inner wall of the chimney. At the same time, the mathematical model of heat and mass transfer of the integrated system is developed, and the feasibility of the designed system is analyzed.

To reduce the height of the collector of SCPPSD, the shallow groove of the closed desalination pool is composed of several annular disc distillation pools with the same radial width in a close arrangement[1]. The cover of the multi-ring plate type distillation pool forms a special oblique-toothed flow channel boundary under the collector, and the oblique-toothed flow channel boundary has a disturbing effect on the flow. Pretorius's scheme was used directly in the convective heat transfer model of the collector in the study of the heat and mass transfer mathematical model of the solar chimney power plant integrated desalination, the influence of the oblique-toothed channel boundary formed by the distillation pool cover on the airflow is also not taken into account. In addition, due to the need for seawater raw materials for the system, the SCPPSD are mostly located in humid environments, and the collector cover may experience nocturnal dewing and sunrise dew evaporation, and there is no study on the dewing effect of SCPPSD.

In order to estimate the system performance more accurately, the influence of the above factors should be taken into account in the calculation model. In this paper, the convective heat transfer mechanism of the collector of SCPPSD, the dewing phenomenon, and the disturbance of the oblique-toothed channel boundary to the hot airflow are considered, the refined mathematical model of unsteady heat and mass transfer was developed, and the effects of nocturnal dewing and humidity on the system performance were discussed. The research in this paper can be used for the performance analysis and design of SCPPSD.

2 Refined Mathematical Model of Heat and Mass Transfer

The structure diagram of the large-scale SCPPSD is shown in Figure 1. The operating principle is shown in[1], which will not be repeated here. The size of SCPPSD is based on the size of the Spanish experimental power plant. The radius of the collector is 122 m, the height is 194.6 m, the radius of the chimney is 5 m, the entrance height of the collector is 2 m, and the exit height is 8 m. Ring-shaped distillation pools are distributed in the collector. The radial length of each ring-shaped distillation pool is 1m, and a total of 117 ring-shaped distillation pools are set.

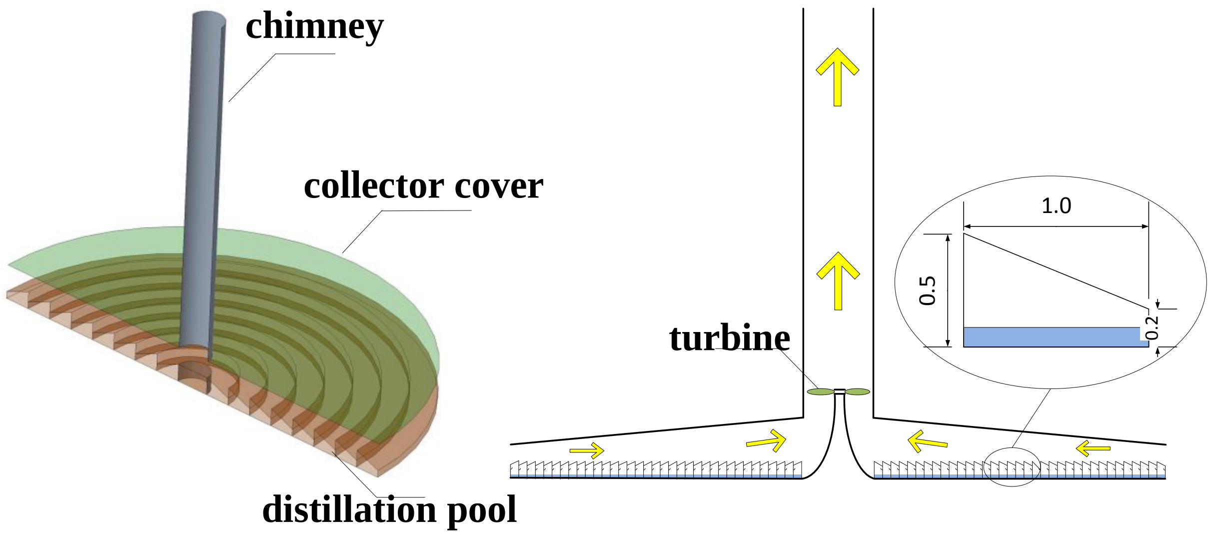

Figure 1. The structure diagram of the large-scale SCPPSD

The mathematical model is developed on the following assumptions:

(1) The airflow flows symmetrically along the radial axis in the collector;

(2) The influence of the solar altitude angle is not considered;

(3) Ignore a series of losses, including various friction losses of air flow and air leakage losses;

(4) The temperature difference in the vertical direction inside the seawater and the airflow is ignored, and seawater and hot airflow are regarded as lumped heat capacity;

(5) Consider the influence of the gear-shaped distillation pool cover on the heat transfer of the hot airflow.

2.1 Meteorological model

Solar radiation is the energy source of the system. The hour-by-hour model of solar radiation S is calculated as follows [25]:

$$S = S_{\max} cos\left[\pi(t - t_{\max}) / D_a\right] \quad (1)$$

Where $S_{\max}$ and $t_{\max}$ are the maximum solar radiation intensity and its corresponding time respectively, and D_a is the day length.

The ambient temperature is calculated as follows[25]:

Daytime:

$$T_a(t) = T_{a,\min} + \Delta T_a \sin\left[\frac{\pi(t - t_{\min})}{D_a + 2a}\right] \quad (2)$$

Nighttime:

$$T_a(t) = (T_{a,\min} - d) + \left[T_{a,set} - (T_{a,\min} - d)\right]\exp\left[\frac{-b(t - t_{set})}{24 - D_a + c}\right] \quad (3)$$

Where $T_{a,\min}$ and $t_{\min}$ are the minimum ambient temperature and its corresponding time respectively, ΔT_a is the daily temperature difference of the ambient temperature, $T_{a,set}$ is the ambient temperature at sunset time t_{set}, a is the difference between the time corresponding to the highest temperature and the time at noon, c is the difference between the sunrise time and the time corresponding to the lowest temperature, b is a constant, the value is 2.2 and d is a parameter set to ensure that the value T_a calculated by equation (3) is equal to $T_{a,\min}$, which is given as follow:

$$d = \left(T_{a,set} - T_{a,\min}\right) / \left[\exp(b) - 1\right] \quad (4)$$

2.2 Unsteady heat transfer model

The energy transfer process in the collector of the integrated system is shown in Figure 2, and the corresponding heat balance equations are as follows:

(1) The collector cover:

$$\alpha_c S(t) + q_{r,gc} = q_{r,cs} + q_{c,ca} + q_{c,cf} + q_{dew} + c_{p,c} M_c \frac{\partial T_c}{\partial t} \tag{5}$$

(2) The air in the collector:

$$q_{c,gf} + q_{c,cf} = c_{p,f} \dot{m}_f \frac{\partial T_f}{\partial r} + c_{p,f} \dot{m}_f \frac{\partial T_f}{\partial t} \tag{6}$$

(3) The distillation pool cover:

$$\alpha_g \tau_c S(t) + q_{c,wg} + q_{r,wg} + q_{ew} = q_{r,cg} + q_{c,gf} + c_{\mathrm{p,g}} M_g \frac{\partial T_g}{\partial \tau} \tag{7}$$

(4) Seawater layer:

$$\alpha_w \tau_c \tau_g S(t) + q_{c,bw} = q_{r,wg} + q_{ew} + q_{c,wg} + c_{p,w} M_w \frac{\partial T_w}{\partial t} \tag{8}$$

(5) The bottom of the distillation pool:

$$\alpha_b \left(1 - \alpha_w\right) \tau_c \tau_g S(t) = q_{c,bw} + q_{kb} + c_{\mathrm{p,b}} M_b \frac{\partial T_b}{\partial \tau} \tag{9}$$

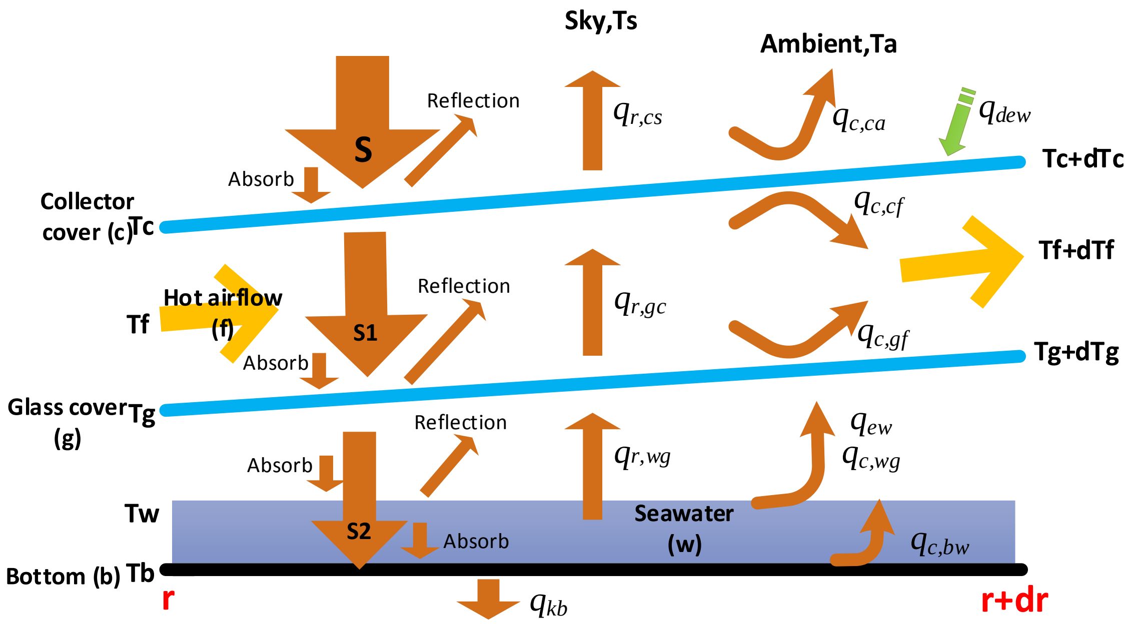

Figure 2. Control body heat transfer process

Each heat transfer rate of formula (5) to formula (9) adopts the following calculation formula:

Radiant heat transfer rate of the collector cover to the sky:

$$q_{r,cs} = \varepsilon_c \sigma [T_c^4 - T_s^4] \tag{10}$$

Sky temperature T_s is calculated from ambient temperature and sky temperature T_s=$0.0552T_a^{1.5}$.

Radiant heat transfer rate of the distillation pool cover to the collector cover:

$$q_{r,gc} = \frac{\sigma(T_g^4 - T_c^4)}{1/\varepsilon_g + 1/\varepsilon_c + 1} \tag{11}$$

Radiant heat transfer rate of seawater surface to the distillation pool cover:

$$q_{r,wg} = \frac{\sigma(T_w^4 - T_g^4)}{1/\varepsilon_w + 1/\varepsilon_g + 1} \tag{12}$$

Convective heat transfer rate between the collector cover and the ambient air:

$$q_{c,ca} = h_{c,ca}\left(T_c - T_a\right) \tag{13}$$

Convective heat transfer rate between the collector cover and the hot airflow:

$$q_{c,cf} = h_{c,cf}\left(T_c - T_f\right) \tag{14}$$

Convective heat transfer rate between the distillation pool cover and the hot airflow:

$$q_{c,gf} = h_{c,gf}\left(T_g - T_f\right) \tag{15}$$

Convective heat transfer rate between seawater and the distillation pool cover:

$$q_{c,wg} = h_{c,wg}\left(T_w - T_g\right) \tag{16}$$

Evaporation heat transfer rate of seawater:

$$q_{ew} = h_{ew}\left(T_w - T_g\right) \tag{17}$$

Heat conduction rate of the bottom of the distillation pool:

$$q_{kb} = U_b\left(T_b - T_a\right) \tag{18}$$

In the SCPPSD system, the convective heat transfer process between the collector cover and hot airflow is regarded as the convective heat transfer process between the hot plate and the gas. According to the study of literature[13], the forms of convection heat transfer are divided into forced convection and natural convection mixed convection heat transfer, and forced convection heat transfer by comparing the collector cover temperature and ambient temperature.

Each heat transfer coefficient from formula (13) to formula (18) is calculated by the following formula.

(1) Convective heat transfer coefficient between the collector cover and the ambient air[13]:

When $T_c > T_a$, The hot side of the collector cover is upward, which is a mixed convection heat transfer mode, $h_{c,ca} = \max\left(h_1, h_2\right)$;

When $T_c < T_a$, The cold side of the collector cover is upward, which is a forced convection heat transfer mode, $h_{c,ca} = h_2$.

Where convective heat transfer coefficient h_1 and h_2 are calculated from:

$$h_1 = \frac{0.2106 + 0.0026v\left(\dfrac{\rho T_m}{\mu g \Delta T}\right)^{1/3}}{\left(\dfrac{\mu T_m}{g \Delta T C_p \lambda^2 \rho^2}\right)^{1/3}} \tag{19}$$

$$h_2 = 3.87 + 0.0022\left(\frac{v \rho C_p}{\Pr^{2/3}}\right) \tag{20}$$

Where v is the ambient wind speed, T_m is the qualitative temperature, ΔT is the temperature difference between the collector cover and air, g is the gravitational acceleration, ρ is the airflow density, μ is the dynamic viscosity, C_p is the specific heat capacity of ambient air at constant pressure, λ is the thermal conductivity of ambient air and Pr is the Prandtl number of the ambient air.

(2) Convective heat transfer coefficient between the collector cover and the hot airflow:

When $T_c > T_f$, the hot side of the collector cover is downward, which is a forced convection heat transfer mode, $h_{c,cf} = \max(h_2, h_3)$;

When $T_c < T_f$, the cold side of the collector cover is downward, which is a mixed convection heat transfer mode, $h_{c,cf} = \max(h_1, h_2, h_3)$.

Where the convective heat transfer coefficient h_3 is given as follows:

$$h_3 = \frac{(f/8)(\mathrm{Re}-1000)\mathrm{Pr}}{1+12.7(f/8)^{1/2}\left(\mathrm{Pr}^{2/3}-1\right)} \frac{\lambda}{d_h} \tag{21}$$

Where f is the Darcy friction coefficient, d_h is the characteristic length, and Re is the Reynolds number.

$$f = (1.82 \lg \mathrm{Re} - 1.64)^{-2} \tag{22}$$

(3) Convective heat transfer coefficient between the distillation pool cover and the hot airflow:

The temperature of the distillation pool cover is always higher than the temperature of the hot airflow[26], which indicates that the distillation pool cover always heats the hot airflow. The heat transfer mode between them is forced convection heat transfer. In the system, the distillation pool cover forms an oblique-toothed flow channel boundary, which is similar to the tooth-shaped channel boundary of the corrugated pipe. So, its heat transfer mode can be regarded as forced convection heat transfer of the corrugated pipe. Due to the vortex flow around the junction of two distillation pools, the flow and heat transfer boundary layer is destroyed, and the convective heat transfer is enhanced. The convection heat transfer between the distillation pool cover and the hot airflow is calculated by the following formula[27]:

$$h_{c,gf} = 0.02313 \mathrm{Re}^{0.8061} \mathrm{Pr}^{1/3} \frac{\lambda}{d_h} \tag{23}$$

(4) Convective heat transfer coefficient between seawater and the distillation pool cover:

$$h_{c,wg} = 0.884 \left[\left(T_w - T_g\right) + \frac{\left(p_w - p_g\right) T_w}{268.9 \times 10^3 - p_w} \right]^{1/3} \tag{24}$$

Seawater evaporation heat transfer coefficient:

$$h_{ew} = 16.273 \times 10^{-3} h_{c,wg} \frac{\left(p_w - p_g\right)}{\left(T_w - T_g\right)} \tag{25}$$

Where p_w and p_g are the water vapor partial pressure of the water surface and distillation pool cover, respectively.

$$p_w = \exp\left(25.317 - \frac{5144}{T_w}\right) \tag{26}$$

$$p_g = \exp\left(25.317 - \frac{5144}{T_g}\right) \tag{27}$$

(5) Convective heat transfer coefficient between the bottom of the distillation pool and seawater[28]:

$$h_{c,bw} = 135 \text{ W/(m}^2 \cdot \text{K)} \tag{28}$$

(6) Thermal resistance of heat conduction of the bottom of the distillation pool[29]:

$$U_b = 14 \text{ W/(m}^2 \cdot \text{K)} \tag{29}$$

2.3 Dewing and dew evaporation model

Zuo et al.[30] found in the test that the temperature of the collector cover of the SCPPSD decreased with the decrease of the ambient temperature at night. When the collector cover temperature drops below the dew point temperature of the ambient air, the water vapor in the air will be separated to the collector cover, and dewing will occur on the surface of the cover. The condensed water on the cover will evaporate, and the heat required for evaporation comes from the collector cover, which makes the collector cover temperature lower than the ambient temperature after midnight. As the hot airflow through the collector cover transfers heat, it may cause the temperature of the hot airflow in this period to be lower than the ambient temperature, thus affecting the power output. Therefore, the influence of dewing on the system performance should be considered in the heat and mass transfer mathematical model of the collector in this paper.

Dewing heat exchange q_{dew} is calculated as follows：

When dew condenses：

$$q_{dew} = h_{con}\left(T_{dew} - T_c\right) \tag{30}$$

Where the condensation heat transfer coefficient is calculated as the following formula[31]：

$$h_{con} = 0.725\left[\frac{gL\rho^2\lambda^3}{\mu l\left(T_{dew} - T_c\right)}\right]^{1/4} \tag{31}$$

Therefore, the quality of condensation is： $M_{con} = q_{dew} / L$, where L is the latent heat of vaporization, l is the characteristic length.

The experimental fitting formula of the maximum water vapor content of the air when the ambient temperature is T [32]is given as follows:

$$f\left(T\right) = 0.00574T^3 - 0.00966T^2 + 0.622T + 4.36 \tag{32}$$

Therefore, the dew point temperature T_{dew} can be solved according to the following equation：

$$f\left(T_{dew}\right) - \varphi_{t\max} f\left(T_{a,\max}\right) = 0 \tag{33}$$

Where $f\left(T_{a,\max}\right)$ is the maximum water vapor content of the air under the highest ambient temperature $T_{a,\max}$， $\varphi_{\min}$ is the relative humidity at the corresponding time, and is also the minimum relative humidity of the whole day.

When dew evaporates:

$$q_{dew} = -M_{eva} \cdot L \tag{34}$$

The dew evaporation rate is calculated as the following formula[33]:

$$M_{eva} = \frac{h_e}{C_{p,a}Le^{2/3}}\left(ds - d\right) \tag{35}$$

h_e is the evaporation heat transfer coefficient, which can be considered as the heat transfer coefficient of air sweeping over the water surface, and is calculated as the following formula[33]:

$$h_e = (0.037\,\mathrm{Re}^{0.8} - 870)\,\mathrm{Pr}^{1/3}\,\frac{\lambda}{d_h} \tag{36}$$

Le is the Lewis number, the value is 0.857[33]. ds and d are the atmospheric moisture content corresponding to dew temperature and ambient temperature, respectively:

$$d = 0.622\,\frac{p_a}{p - p_a} \tag{37}$$

$$p_a = RH \cdot p_{sv} \tag{38}$$

$$p_{sv} = 608.2 \cdot 10^{8.5(T-273.15)/T} \tag{39}$$

Where p_{sv} is the saturated water vapor pressure, p is the standard atmospheric pressure, RH is the relative humidity of the air, RH at time t is calculated as the following formula:

$$RH(t) = \frac{\varphi_{\min} f\left(T_{a,\max}\right)}{f\left(T_a(t)\right)} \tag{40}$$

The dew quality M_{dew} on the collector cover surface at time t is calculated as the following formula:

$$M_{dew} = \int_{t_a}^{t} \left(M_{con} - M_{eva}\right) \tag{41}$$

Where t_a is the calculation start time. According to the research in literature[34], if the dew of the collector cover hasn't completely evaporated after sunrise, the dew of the cover will also affect its light transmittance. Therefore, the light transmittance of the collector cover τ_c will change to $\tau_c\left(1-\alpha_w\right)$ when there is dew.

2.4 System performance calculation model

Hot airflow velocity at the chimney inlet:

$$v_{in} = \sqrt{2gH_{ch}\frac{\Delta T}{T_a}} \tag{42}$$

Water production ratio:

$$m_e = q_{ew} / L \tag{43}$$

Output power of the system：

$$P_e = \frac{1}{3}\eta_{tur}\rho_{air}A_{ch}v_{in}^3 \tag{44}$$

Daily utilization efficiency of solar energy：

$$\eta_s = \frac{\sum P_e + \sum m_e \cdot L}{\sum S \cdot A_{col}} \tag{45}$$

3 Numerical solution and verification of the model

3.1 Equation discretization and solution

All differential terms in the control equation are discretized by backward difference. . A diagram of the discrete nodes of space and time for SCPPSD is shown in Figure 3

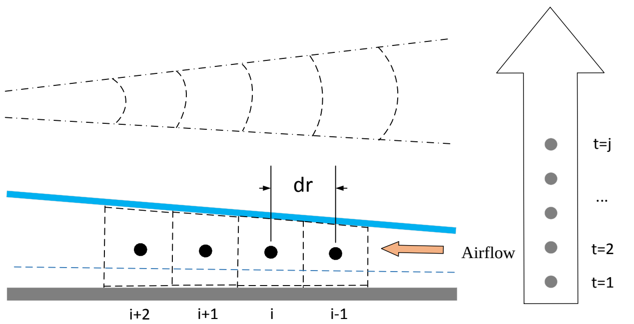

Figure 3. Discrete diagram of nodes in SCPPSD system

The equations in discrete form:

$$\alpha_c S(t) + q_{r,gc} = q_{r,cs} + q_{c,ca} + q_{c,cf} + q_{dew} + c_{p,c} M_c \frac{T_{c,i}{}^{j} - T_{c,i}{}^{j-1}}{\Delta t} \tag{46}$$

$$q_{c,gf} + q_{c,cf} = c_{p,f}\dot{m}_f \frac{T_{f,i} - T_{f,i-1}}{dr} + c_{p,f}\dot{m}_f \frac{T_{f,i}{}^{j} - T_{f,i}{}^{j-1}}{\Delta t} \tag{47}$$

$$\alpha_g \tau_c S(t) + q_{c,wg} + q_{r,wg} + q_{ew} = q_{r,cg} + q_{c,gf} + c_{p,g} M_g \frac{T_{g,i}{}^{j} - T_{g,i}{}^{j-1}}{\Delta t} \tag{48}$$

$$\alpha_w \tau_c \tau_g S(t) + q_{c,bw} = q_{r,wg} + q_{ew} + q_{c,wg} + c_{p,w} M_w \frac{T_{w,i}{}^{j} - T_{w,i}{}^{j-1}}{\Delta t} \tag{49}$$

$$\alpha_b\left(1-\alpha_w\right)\tau_c\tau_g S(t)=q_{c,bw}+q_{kb}+c_{\mathrm{p,b}}M_b\frac{T_{b,i}{}^{\mathrm{j}}-T_{b,i}{}^{\mathrm{j\text{-}1}}}{\Delta t} \tag{50}$$

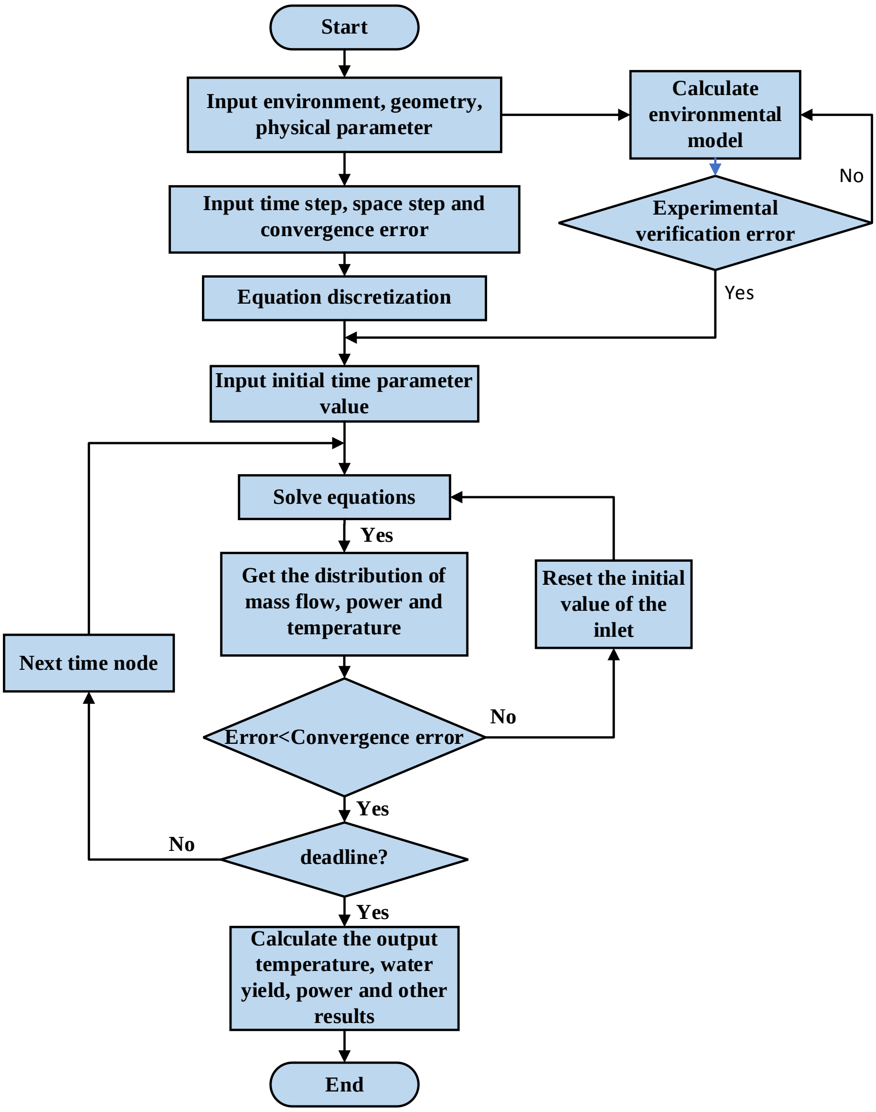

Figure 4. Flow chart of numerical solution

The numerical solution flow chart of the mathematical model is shown in Figure 4. Set the time step to 5 minutes. The specific solution idea is: at time t, the heat and mass transfer equations are solved step by step along the radial direction of the control volume from the inlet by giving the inlet boundary conditions. The boundary conditions of the control volume r+dr are provided by the solution of the r control volume equations, which makes the equations of the control volume r+dr closed and ensures that the equations were solved successfully. After solving the heat and mass transfer equations in the collector area, the temperature, pressure, air velocity, and other parameters in the system at time t are obtained. Through the performance calculation model, the mass flow rate and output power of the system are obtained. If the mass flow rate meets the convergence conditions, the equations at t time are solved; otherwise, reset the inlet wind speed, iteratively solve the heat and mass transfer equations of the collector until the mass flow rate meets the convergence conditions, then solve the next time node, and finally simulate the all-weather operation of the system.

3.2 Model validation

In order to verify the correctness and rationality of the developed refined mathematical model of heat and mass transfer of SCPPSD, the structural parameters of the physical model use the basic structural dimensions of the small SCPPSD test device, as shown in Figure 5. At this time, the seawater thickness in the distillation pool is 8 cm, and the details of the test device are shown in the literature[26]. The meteorological conditions are the climatic conditions[26] measured on the test day of August 1, 2021. The mathematical model is solved by self-programming MATLAB program, and the calculation results are compared with the test results[26].

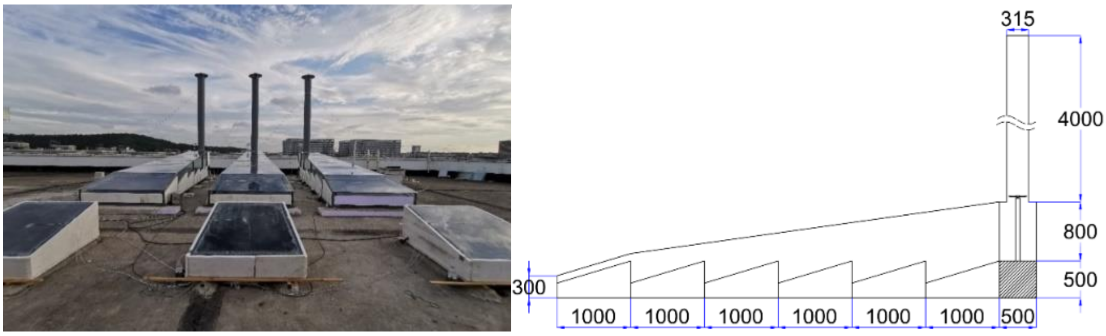

Figure 5. Small SCPPSD test apparatus and dimensions

The validity of the comparison between the numerical calculation results x_i and the test results y_i can be expressed by the correlation coefficient r [35]:

$$r = \frac{N\sum_{i=1}^{N} x_i y_i - \sum_{i=1}^{N} x_i \sum_{i=1}^{N} y_i}{\sqrt{N\sum_{i=1}^{N} x_i^2 - \left(\sum_{i=1}^{N} x_i\right)^2}\sqrt{N\sum_{i=1}^{N} y_i^2 - \left(\sum_{i=1}^{N} y_i\right)^2}} \tag{51}$$

The closeness between numerical calculation results and test results can be expressed by the root mean square of percentage deviation e:

$$e = \sqrt{\frac{\sum_{i=1}^{N}\left(\frac{x_i - y_i}{x_i}\right)^2}{N}} \tag{52}$$

Figure 6(a)~(j) shows the comparison curves between the test results and numerical calculation results of solar irradiance, ambient temperature, ambient humidity, collector cover temperature, hot airflow temperature, distillation pool cover temperature, seawater temperature, hourly water yield per unit area, chimney inlet air temperature and velocity on the test day. Table 1 shows the summary of statistical analysis of the comparison between the test results corresponding to Figure 6 and the numerical calculated results. It can be seen from Figure 6(a) that the solar irradiance obtained by the calculation model is a cosine change during the day, which can more accurately reflect the change rule of solar irradiance on the test day. It can be seen from Table 1 the correlation coefficient between the calculated solar irradiance and the test value is as high as 95.0%. However, it can be seen from Table 1 that the error of the solar irradiance calculation model is very large, which is 28.7%. The main reason is that the deterministic solar irradiance model is adopted in this paper, and the randomness of solar irradiance changes is ignored. The ambient temperature calculation model has high accuracy. Its correlation coefficient with the test value is 98.0%, and the error with the test value is 2.04%. The minimum error of the mathematical model used in the literature[18] is 2.7%. Compared with the model in the literature[18], the accuracy of the ambient temperature calculation model in this paper is higher, as shown in Figure 6(b). Similarly, the correlation coefficient between the calculated value of ambient relative humidity and the test value is 95.0%, and the error between them is 7.54%, which can better describe the changing trend of ambient humidity.

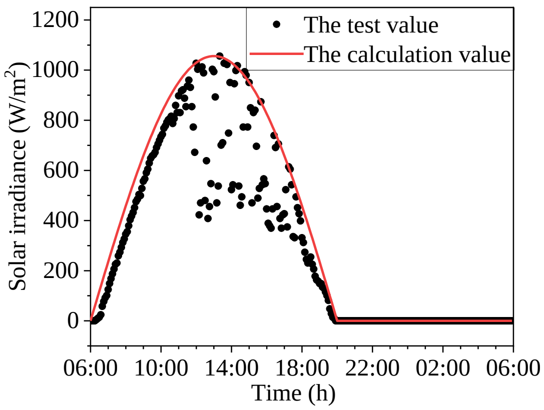

(a) Solar irradiance

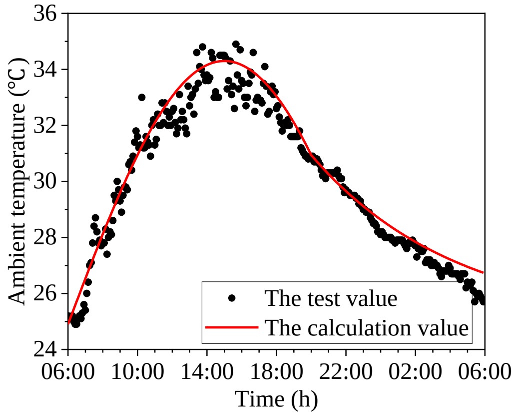

(b) Ambient temperature

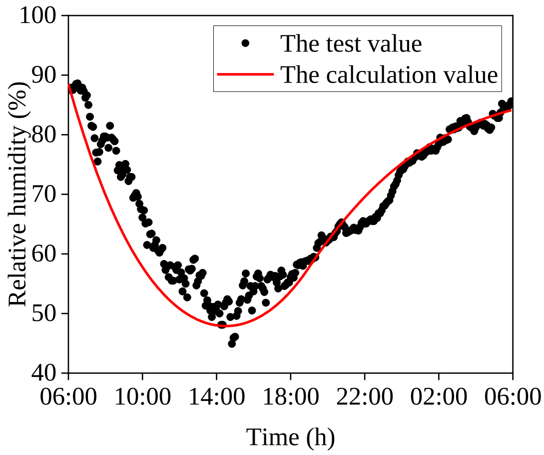

(c) Ambient relative humidity

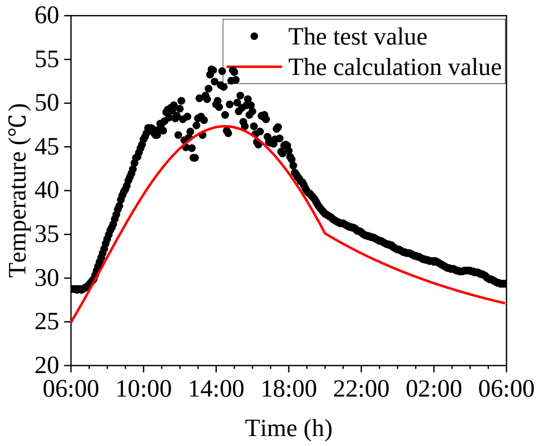

(d) Collector cover temperature

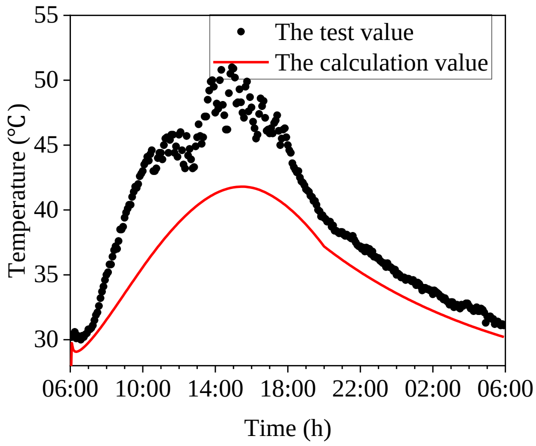

(e) Hot airflow temperature in the middle section of the collector

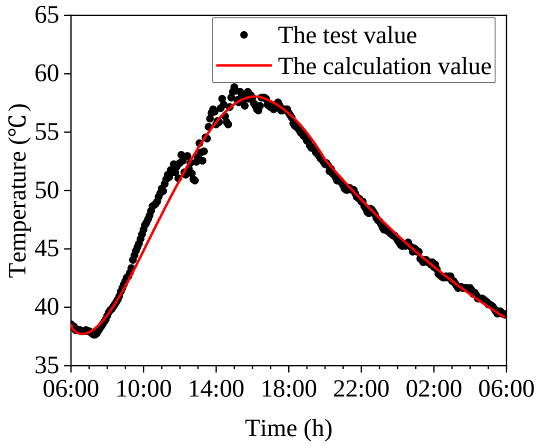

(f) Distillation pool cover temperature

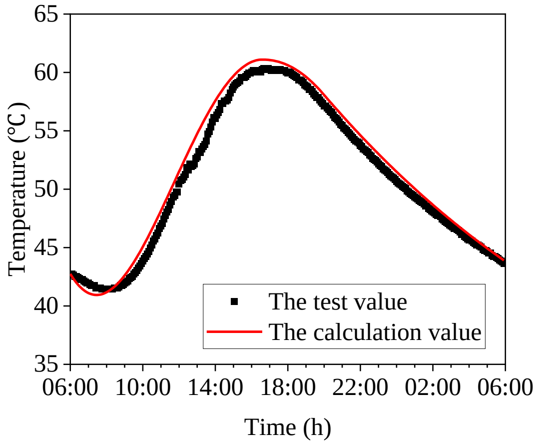

(g) Seawater temperature

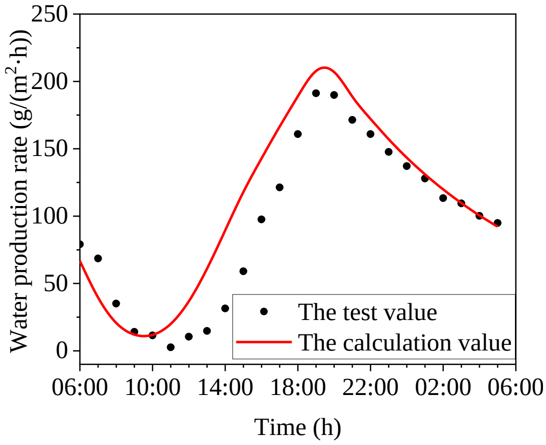

(h) Hourly water yield per unit area

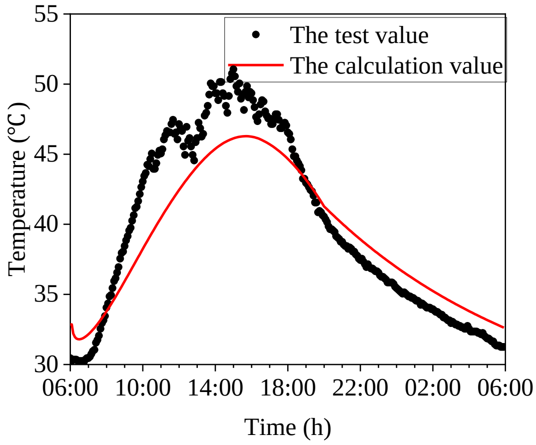

(i) Airflow temperature at chimney inlet

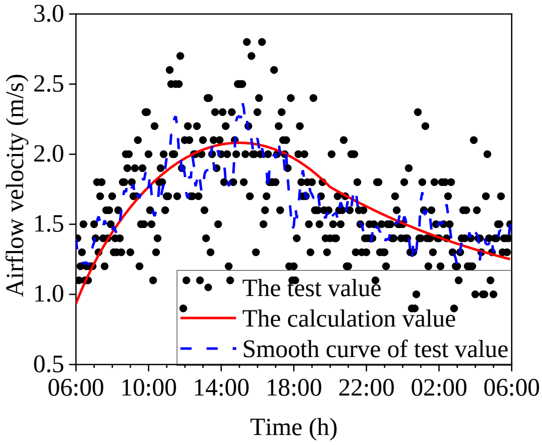

(j) Airflow velocity at chimney inlet

Figure 6. Comparison curves between test results and numerical calculation results

Table 1 Statistical analysis of the comparison between test results and calculation results

Physical quantity	the correlation coefficient r (%)	the root mean square e (%)
(a)Solar irradiance	95.0	28.7
(b)Ambient temperature	98.0	2.04
(c)Ambient humidity	95.0	7.54
(d)Collector cover temperature	97.9	7.49
(e)Hot airflow temperature in the middle section of the collector	95.8	9.83
(f)Distillation pool cover temperature	99.3	1.56
(g)Seawater temperature	99.7	1.78
(h)Hourly water yield per unit area	93.4	39.9
(i)Airflow temperature at chimney inlet	95.7	5.70
(j)Airflow velocity at chimney inlet	55.7	20.1

It can be seen from Figure 6 and Table 1 that the correlation coefficient between the calculated value of each physical quantity and the test value is greater than 90%, except for the airflow velocity at the chimney inlet. The mathematical model developed in this paper can accurately reflect and evaluate the changes in the operating characteristics and output characteristics of SCPPSD. The calculation of seawater temperature and distillation pool cover temperature is more accurate, and the best agreement with the test curve, as shown in Figure 6(g)and(f), with root mean square error of 1.78% and 1.56% respectively. The temperature of the hot airflow in the collector calculated by the numerical method is obviously lower than the test value, and the error with the test value is 9.83%. The main reason is that the side panel of the test device will also heat the airflow during the daytime. In large SCPPSD, the collector is circular and there is no side panel, so there is no side panel heating. The control volume in this mathematical model calculation does not consider the side panel heating effect. The decrease of the calculated value of the hot airflow temperature in the collector also leads to the smaller calculated value of the collector cover temperature, and the error of the collector cover temperature is 7.49%, which is slightly smaller than the error of the temperature of the hot airflow in the collector.

The root means square error between the calculated value of hourly water yield per unit area and the test value is 39.9%, with a large error. It can be seen from Figure 6(h) that the calculated value of hourly water yield per unit area is relatively large in the rising section of water yield. The main reasons are: (1) Some condensed distilled water on the inside of the glass cover may drip back to the distilling pool when they flow to the collecting tank, resulting in a relatively small water yield in the test. (2) The calculation model does not consider the inclination angle of the collector cover. Horizontal solar radiation is adopted, while the actual cover has a certain inclination.

Because the loss rate of the power generation device in the test device is large, and the difference between the calculated power of the model and the measured power is large, the airflow temperature and velocity at the chimney inlet are used for verification. According to formulas (42) and (44), when the size of SCPPSD is determined, the system output power is mainly determined by the temperature rise of the hot airflow at the chimney inlet relative to the external ambient temperature, that is, the output power is mainly determined by the temperature of the hot airflow at the chimney inlet. It can be seen from Table 1 that the correlation coefficient between the chimney inlet airflow temperature calculated by the proposed model and the test value is 95.7%, and the root mean square error is 5.70%, indicating that the proposed mathematical model can accurately calculate the output power characteristics of the system. Because of the great fluctuation of the test data of the airflow velocity at the chimney inlet, the correlation coefficient between the calculated value and the test value is very low, and the error between them is as high as 20.1%. However, it can be seen from the comparison between the smooth curve of the airflow velocity test value at the chimney inlet and the calculated value curve that the changing trend of the proposed mathematical model is close to that of the smooth curve of the airflow velocity test value in the chimney, which can be used to describe the power output of SCPPSD.

Figure 7 shows the radial distribution curve of the temperature of the collector cover, the airflow, the seawater, and the distillation pool cover at different times. It can also be seen from the radial distribution curve that the calculation of seawater temperature and distillation pool cover temperature are in the best agreement with the test curve, followed by the collector cover temperature , and the numerical calculation of the hot airflow temperature deviates greatly from the test curve, indicating that in addition to the influence of the side wall heating effect of the test device mentioned above, the radiation intensity, radiation time and other environmental factors (environmental temperature, wind speed, etc.), seawater temperature, water vapor condensation, condensate collection under the distillation pool cover, collector materials, and heat collection performance will have a certain impact on the temperature and temperature rise of the hot airflow.

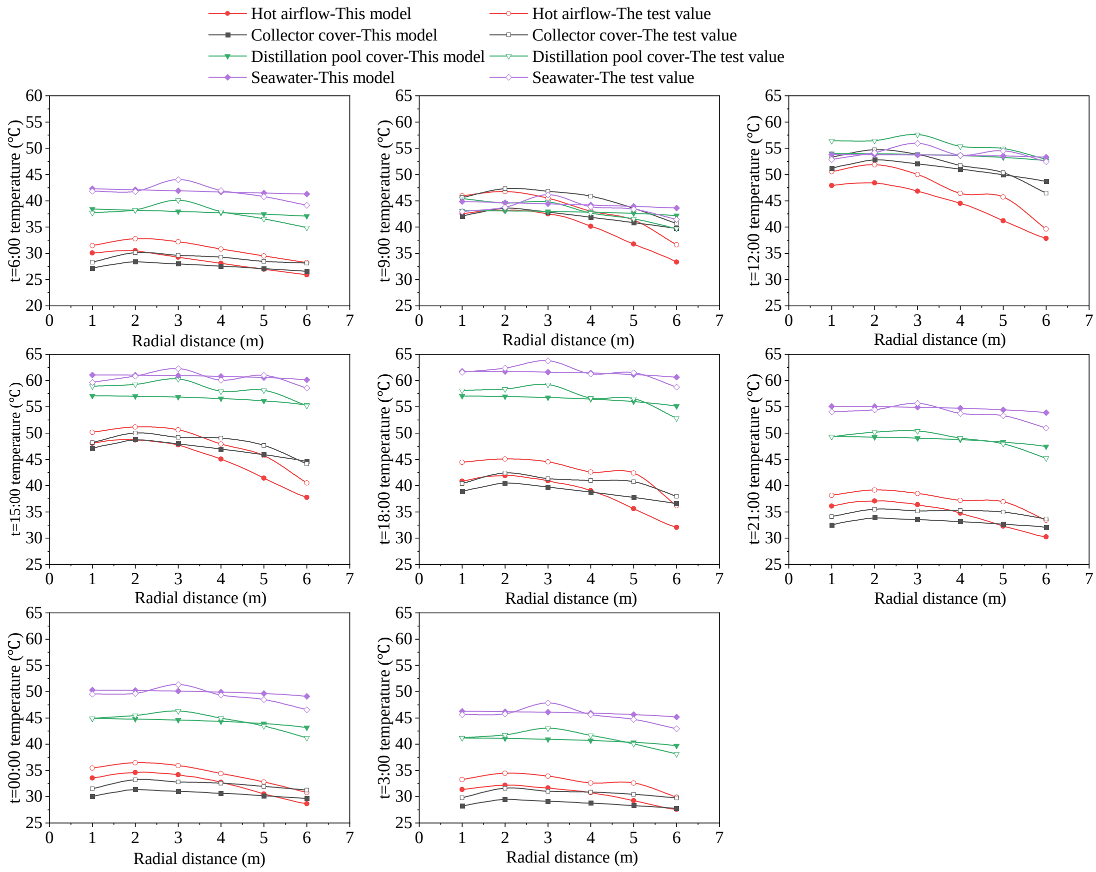

Figure 7. Radial temperature distribution curves at different times

The difference between the mathematical model in this paper and the original mathematical model [18], and the comparison between the calculated results of the two models and the test results are shown in the Appendix.

4 Comparison of heat transfer coefficient schemes with or without considering the effect of oblique-toothed flow channel boundary

For the convection heat transfer coefficient between the distillation pool cover and the hot airflow, the calculation model in the previous literature[18] used the Gnielinski formula, i.e., $h=\frac{(f/8)(\mathrm{Re}-1000)\mathrm{Pr}}{1+12.7(f/8)^{1/2}\left(\mathrm{Pr}^{2/3}-1\right)}\frac{\lambda}{d_h}$, which is applicable to the forced convection heat transfer in the tube but did not consider the disturbance to the airflow caused by the oblique-toothed flow channel boundary formed by the distillation pool cover in the collector. The calculation model in literature [18] has been revised in the model scheme in this paper, in which the convection heat transfer coefficient between the distillation pool cover and the hot airflow adopts the forced convection heat transfer coefficient of the corrugated pipe with an internal serrated channel surface, i.e, equation (23) $h = 0.02313\,\mathrm{Re}^{0.8061}\,\mathrm{Pr}^{1/3}\,\dfrac{\lambda}{d_h}$, which is close to the boundary of the oblique-toothed flow channel, to consider the disturbance effect of the oblique-toothed flow channel boundary on the airflow.

In order to compare the difference between the calculation results under the two heat transfer coefficient schemes, and to facilitate the comparison with the test results, the structural parameters in the two calculation models uniformly adopt the basic structural dimensions of the small SCPPSD test device shown in Figure 5. The meteorological conditions are still the climatic conditions measured on the test day of August 1, 2021 [26]. In the two calculation models, only the convective heat transfer coefficient schemes between the distillation cover and the hot airflow are different. In the complete numerical calculation model built in this paper, it is called the original heat transfer coefficient scheme if the Gnielinski formula is used in the convection heat transfer coefficient between the distillation cover and the hot airflow, and is called this heat transfer coefficient scheme if the forced convection heat transfer coefficient of the corrugated pipe is used.

Figure 8 shows the comparison between the test data and calculation results which adopt the convection heat transfer coefficient scheme of this model and the original model, respectively. Table 2 shows the error analysis between the numerical calculation values and the test values of the two heat transfer coefficient schemes corresponding to Figure 8. Because the airflow velocity in the chimney in the test fluctuates too much, the airflow temperature at the chimney inlet is used for comparison. It can be seen from Figure 8 that the convective heat transfer coefficient between the distillation pool cover and the hot airflow $h_{c,gf}$ has the greatest influence on the seawater temperature and the distillation pool cover temperature, and the seawater temperature and the distillation pool cover temperature calculated with the original heat transfer coefficient scheme are both greater than calculated with this scheme and the test values, as shown in Figure 8(d) and Figure 8(c). Combined with the error value in Table 2 that the seawater temperature and the distillation pool cover temperature calculated by this scheme are more accurate than that calculated by the original scheme.

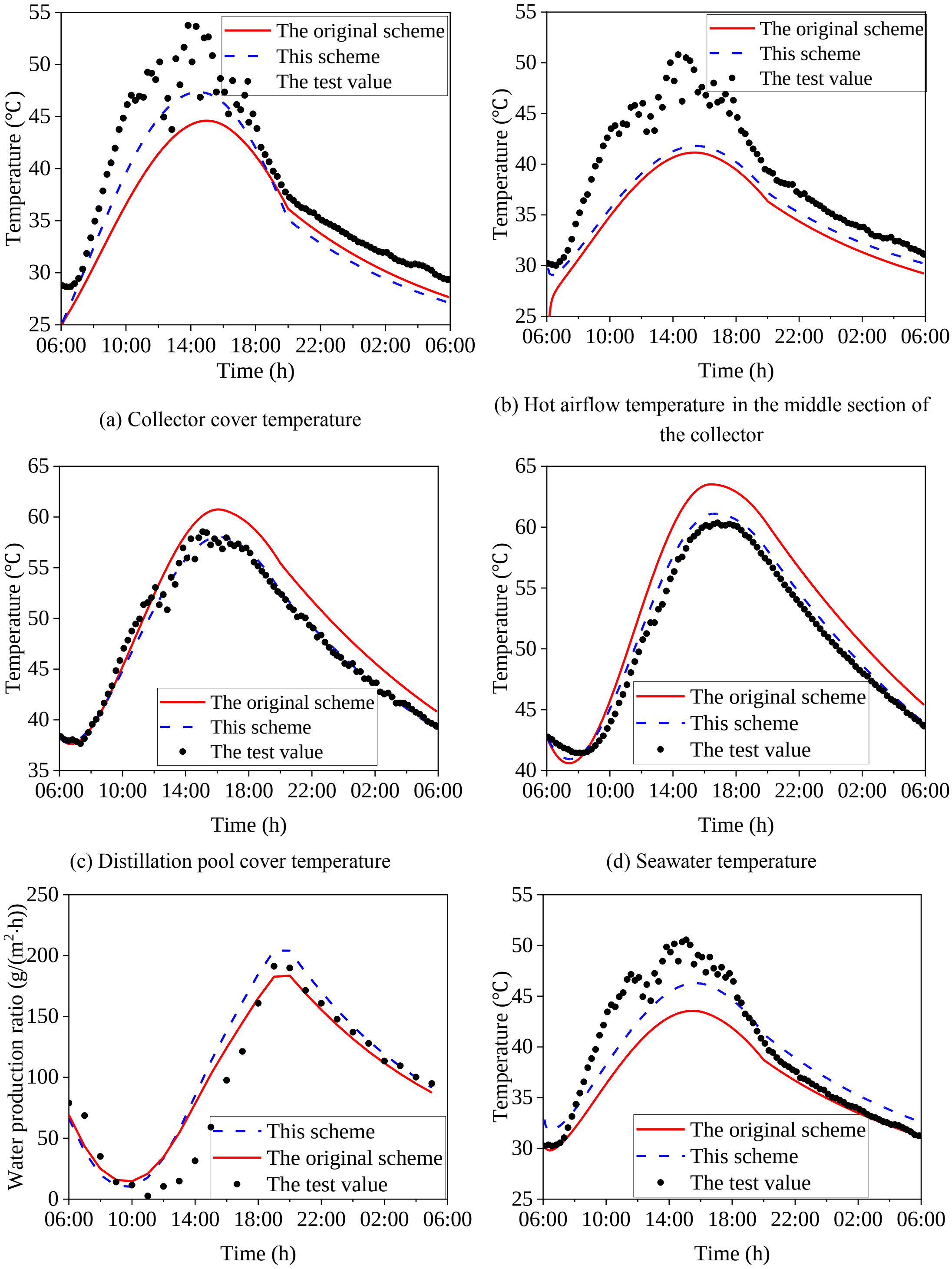

(a) Collector cover temperature

(b) Hot airflow temperature in the middle section of the collector

(c) Distillation pool cover temperature

(d) Seawater temperature

(e) Water production ratio

(f) Airflow temperature at chimney inlet

Figure 8. Effect of convective heat transfer coefficient scheme

Figure 10 shows that $h_{c,gf}$ changes with the airflow speed. It can be seen from Figure 10 that after taking into account the oblique-toothed flow channel boundary of the distillation pool cover, the heat transfer coefficient of the distillation pool cover and the hot airflow in the collector is greater than that of the original heat transfer coefficient scheme, which increases the heat exchange between the hot airflow and the distillation pool cover, resulting in more heat dissipation of the seawater and the distillation pool cover, and more heat absorption by the airflow. As shown in Figure 8(b), the airflow temperature in the collector is higher than that in the original scheme and closer to the test value. As a result, the airflow temperature at the chimney inlet is also higher than that of the original scheme. It can be seen from Figure 8(f) that the airflow temperature at the chimney inlet calculated by the original scheme is too small, which will cause a lower estimation of the system output power.

For the collector cover, the calculated value of the convective heat transfer coefficient between the collector cover and the external environment $h_{c,ca}$ in this heat transfer coefficient scheme is 12.02 W/(m^2·K); In the original scheme is 10.2 W/(m^2·K). However, the temperature of hot airflow in the collector in this scheme is higher, and the heat transfer coefficient between the hot airflow and the cover is also higher during the daytime. Therefore, even though $h_{c,ca}$ in this scheme is larger, the daytime collector cover temperature calculated by this scheme is still higher than that calculated by the original scheme, as shown in Figure 8(a). However, after sunset, the temperature of the hot airflow in the collector decreases, the speed decreases, the heat transfer coefficient between the hot airflow and the collector cover also decreases, and the collector cover has greater external heat dissipation, which leads to the collector cover temperature calculated by this scheme is smaller than by the original scheme at night. Based on the above analysis, the convection heat transfer between the collector cover and the external environment calculated by the original scheme is smaller than that calculated by this scheme, which ultimately leads to the high deviation of the collector cover temperature from the test value.

It can be seen from Figure 8(e) that the hourly water yield per unit area calculated by this heat transfer coefficient scheme is generally larger than by the original heat transfer coefficient scheme, and only slightly smaller than calculated by the original scheme during 8:00-12:00. the temperature difference between the seawater and distillation pool cover of the original scheme is larger during 8:00-12:00 (As shown in Figure 9), and the water production rate is positively correlated with the temperature difference, which leads to higher water production ratio of the original scheme during this period. With the increase in seawater temperature, the temperature difference between the seawater and distillation pool cover in this scheme gradually exceeds that in the original scheme, which result in the water production rate in this scheme also exceeds that in the original scheme. At the peak value of the water production ratio, the difference between the temperature difference between the seawater and the distillation pool cover in this scheme and in the original scheme reaches the maximum, and the difference between the water production rate in this scheme and the water production rate in the original scheme also reaches the maximum. In the water yield decline section, the temperature difference between the seawater and distillation pool cover in the two schemes both decrease gradually, but the seawater temperature in the original scheme is higher (As shown in Figure 8(d)), so the decline of the water production ratio in the original scheme is smaller than that in this scheme, which leads to the gradual approximation of the water production ratio of the two schemes.

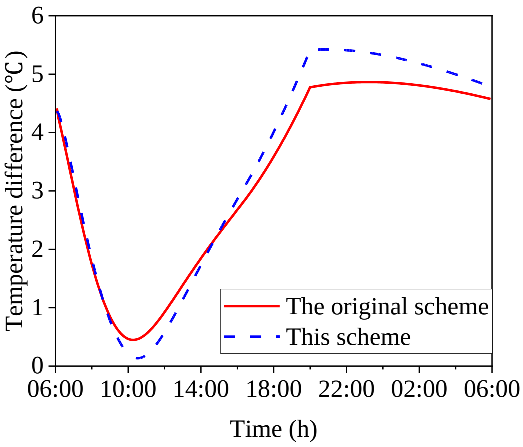

Figure 9. The temperature difference between the seawater and the distillation pool cover

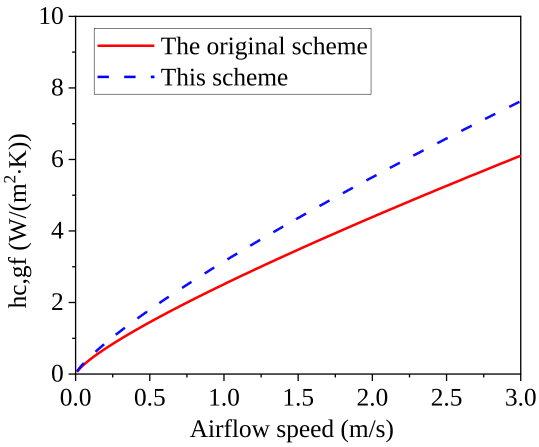

Figure 10. Convective heat transfer coefficient between the distillation pool cover and the hot airflow

In conclusion, combined with Table 2, it can be seen that the calculated temperature values of the collector cover, the hot airflow in the collector, the distillation pool cover, the seawater, and the hot airflow in the chimney of the heat transfer coefficient scheme in this paper have smaller errors with the test values, and the error of the hourly water yield per unit area is close to the original heat transfer coefficient scheme, which shows that the heat transfer coefficient scheme adopted in this model, which takes into account the influence of the oblique-toothed flow channel boundary, is more accurate for the performance calculation of SCPPSD.

Table 2 Error analysis of the test results and the calculated values of two schemes

Physical quantity	This scheme *e* (%)	Original scheme *e* (%)
(a)Collector cover temperature	7.49	9.79
(b)Hot airflow temperature in the middle section of the collector	9.83	11.8
(c)Distillation pool cover temperature	1.56	4.53
(d)Seawater temperature	1.78	5.04
(e)Hourly water yield per unit area	39.9	39.3
(f)Airflow temperature at chimney inlet	5.70	9.58

5 Study on the influence of humid environment and the dewing occurred on the collector cover surface

5.1 Influence of dewing at night

Based on the above mathematical model and the data of solar radiation and ambient temperature and humidity from the test in literature[34], the impact of dewing in a high-humidity environment on the system performance of large SCPPSD is explored.

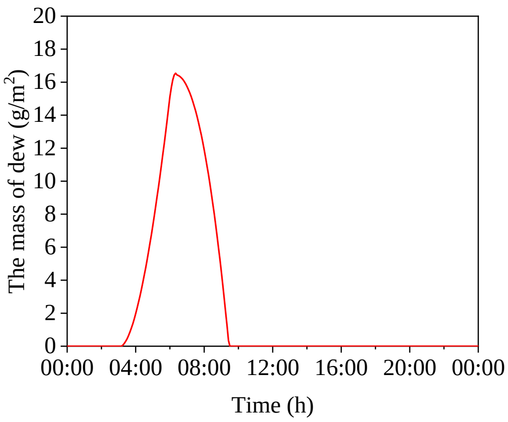

Figure 11. The change curve of dew quality

Figure 11 shows the change curve of dew mass per unit area of the collector cover. It can be seen from the figure that due to the low system temperature at the initial time, the phenomenon of rapid dewing occurred, and the dew gradually evaporated as the collector cover temperature increased. The dewing on the first day of calculation starts at 3:50, and then the dew on the collector cover gradually increases to the maximum at

6:25. The total mass of dew on the collector cover is about 16.5 g/m^2. As the collector cover temperature gradually rises after sunrise, the dew on the collector cover evaporates. By 9:25, all the dew evaporates, and the evaporation time is about 3h. According to the test data in the literature[34], the starting time of dewing of the collector cover is 2:00 to 3:00, the ending time of dewing is 6:00 to 6:30, the evaporation time of dew is about 2-3 hours, and the dew quality of the collector cover is 10-25 g/m^2. The dew evaporation period and dew quality calculated in this paper are close to the test results, indicating the reliability of the dewing model calculation in this paper.

Figure 12 shows the temperature change curve of the system with or without considering night dewing and sunrise dew removal. It can be seen from Figure 12(a) that the collector cover temperature during the dewing period is higher than that in without considering dewing model due to the heat release of dew condensation, while the collector cover temperature decreases after the sunrise due to the heat absorption of dew evaporation, and the influence continues. The collector cover temperature is always lower than that in without considering dewing model in the subsequent period. The influence of dewing and dew removal on the changing trend of the hot airflow temperature is the same as that on the collector cover. It can be found that dewing exothermic slightly increases the hot airflow temperature, while dew evaporation endothermic also decreases the hot airflow temperature throughout the day. It can be seen from Figure 12(c) and Figure 12(d) that the dewing process has little impact on the temperature of the seawater and the distillation pool cover. The temperature of the seawater and the distillation pool cover calculated by the two models are almost equal at 2:00-6:30, but the temperature of the seawater and the distillation pool cover decrease during dew evaporation. This is because the heat released and absorbed by dew condensation or dew evaporation process is small, which is not enough to affect the seawater temperature. However, dew will reduce the light transmittance of the collector cover, playing the same shielding role as sand and dust, reducing the solar energy absorbed by the system, causing the temperature of the seawater and the distillation pool cover to drop.

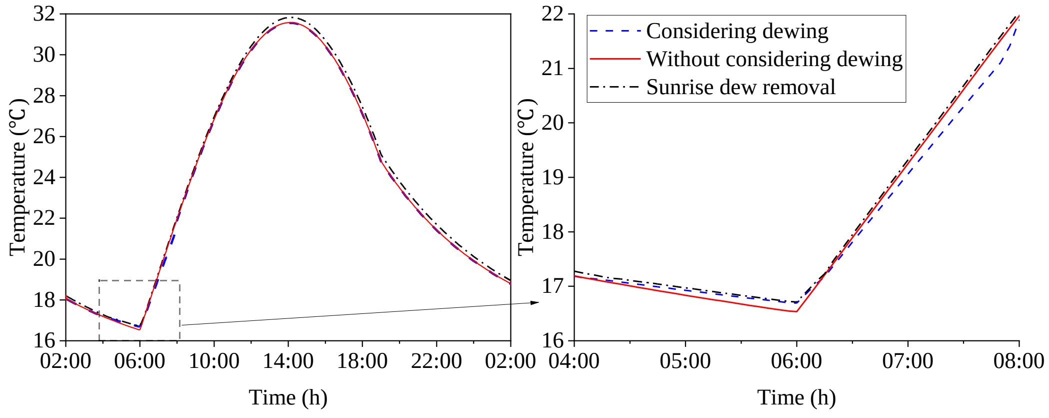

(a) Collector cover temperature

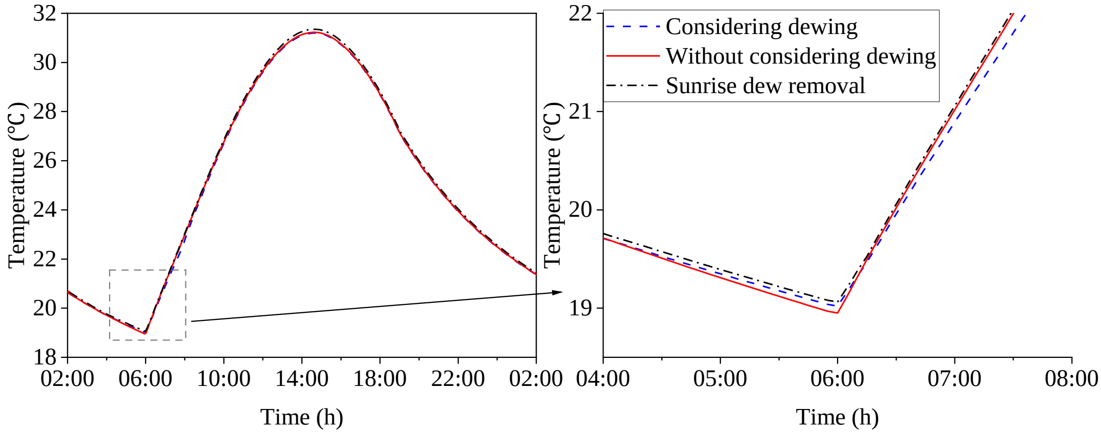

(b) Hot airflow temperature

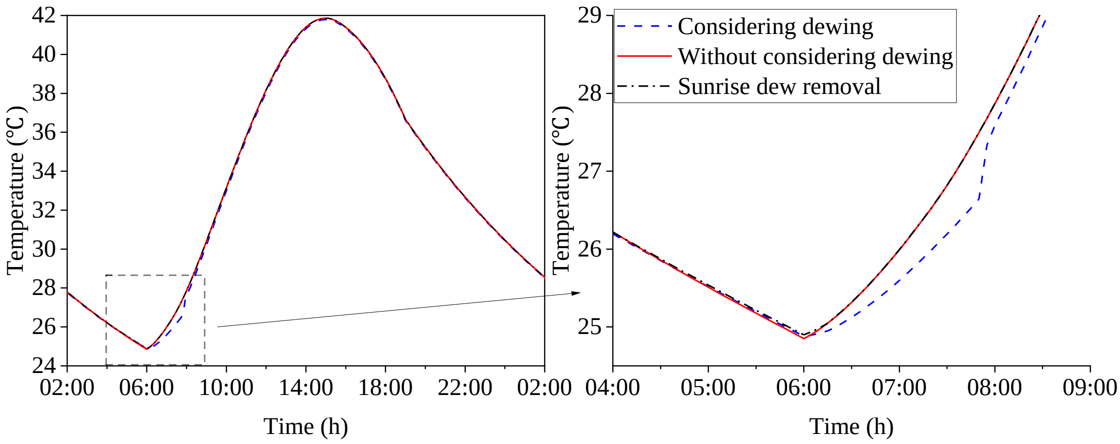

(c) Distillation pool cover temperature

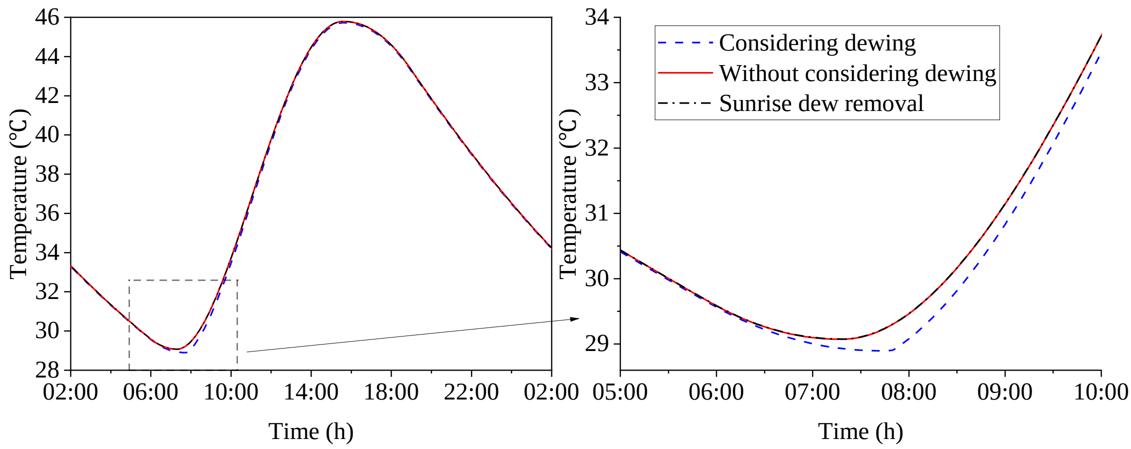

(d) Seawater temperature

Figure 12. Effect of dewing on the temperature

Figure 13 shows the influence of dewing on the water production ratio and power output of the system. It can be seen from Figure 13(b) that dewing has little impact on the output power of the system, so the impact of sunrise dew removal on the output power of the system is not considered. This is because the collector of large SCPPSD has a large radius, the airflow temperature in the collector near the chimney is high, the collector cover temperature is high, the mass of dew is small, and the dewing has little impact on the temperature rise of the system, thus having little impact on the output power. It can be seen from Figure 13(a) that, for the water production ratio, the hourly water yield per unit area of the system during the dewing period is almost the same as that without dewing, while the dew during the dew evaporation period will cause the system water production ratio to decline, and the sunrise dew removal measures can weaken this negative effect. In large SCPPSD, the distilling pool is arranged under the whole collector. The closer the distilling pool is to the inlet area of the collector, the lower the airflow temperature is, and the greater the possibility of dewing on the collector cover. Because the dew reduces the light transmittance of the collector cover, which will affect the absorption of solar radiation energy by seawater and then affect the rise of seawater temperature, the system water production ratio during the dew evaporation period will be reduced compared with that without considering dewing.

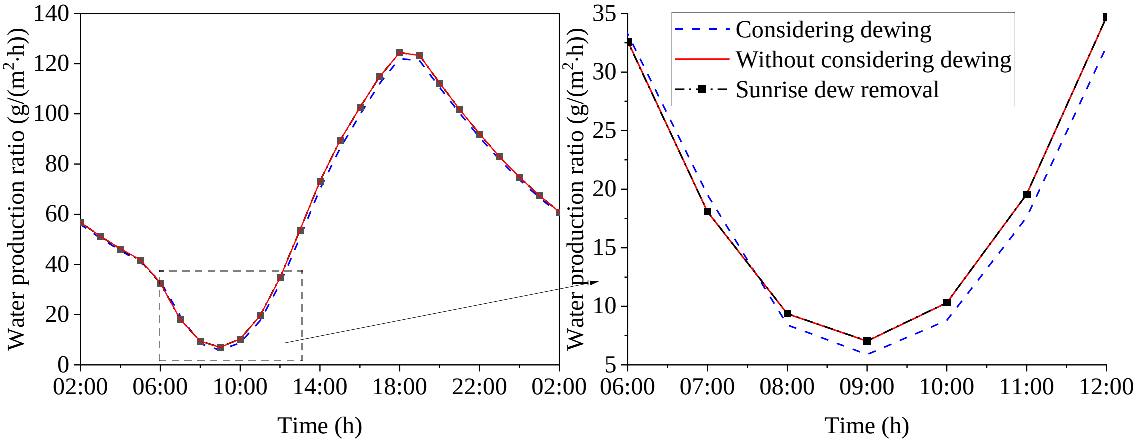

(a) Water production ratio

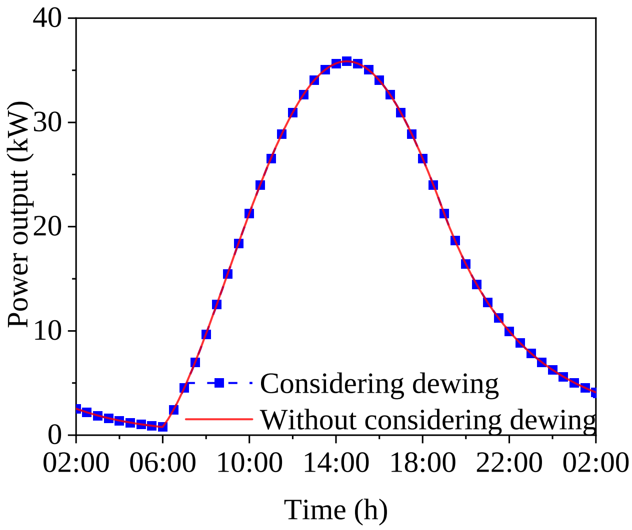

(b) Power output

Figure 13. Effect of cover dewing on water production ratio and power generation

According to the calculation, the daily utilization efficiency of solar energy without considering the cover dewing, considering dewing, and sunrise dew removal is 27.42%, 27.15%, and 27.43% respectively. The impact of dewing is not obvious, and the sunrise dew removal even makes the utilization efficiency higher than that without considering dewing.

The above research results show that for SCPPSD, due to the good effect of seawater heat storage at night, the collector cover temperature decreases at night, but the mass of dew is small, and the impact of dewing on the system performance is small, indicating that SCPPSD coupled with SCPP and disc distillation pool has a better anti-dewing negative impact characteristic.

5.2 Impact of ambient humidity

The ambient humidity has a decisive effect on whether dewing will occur. Dewing is very likely to occur on the collector cover in the high humidity environment, while it is generally difficult to occur in high temperature and dry environments. Generally, when the ambient temperature is the highest, the ambient humidity is the lowest.

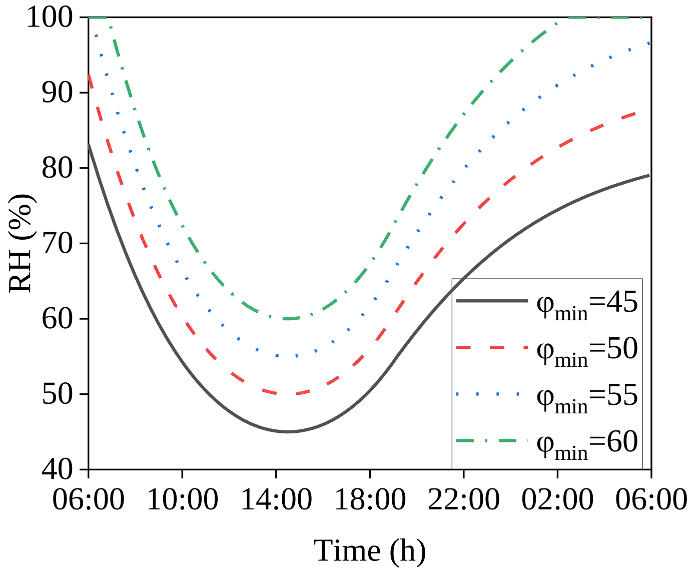

Figure 14. Change of relative humidity with time

The minimum ambient humidity $\varphi_{\min}$ is set at 45%, 50%, 55%, and 60% respectively to explore the influence of ambient humidity on dewing and system performance. Figure 14 shows the change of ambient relative humidity with time under different $\varphi_{\min}$ conditions. It can be seen from the figure that when $\varphi_{\min}$ is 45%, the maximum value of *RH* is 83%; When $\varphi_{\min}$ is 60%, *RH* reaches 100% at 2:25-6:50, the water vapor in the air reaches supersaturation, and the water vapor condenses. There may be rainfall. It can be seen that 60% is already very wet, so the larger $\varphi_{\min}$ is not considered.

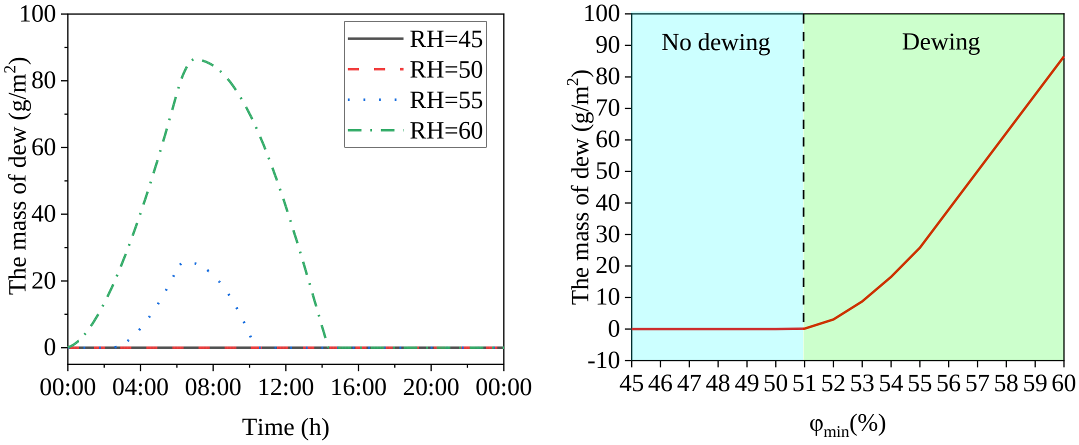

(a) The mass of dew changes with time

(b) The mass of dew changes with minimum humidity

Figure 15. Effect of relative humidity on dewing

Figure 15 shows the mass of dew changes under different humidity. It can be seen from Figure 15(a) that when the relative humidity is less than 50%, there is no dew on the surface of the collector cover, and the critical humidity for generating dew is between 50% and 55%. However, when φ_{min} increases from 55% to 60%, the mass of dew increased from 25.8 g/m^2 to 86.5 g/m^2, an increase of 235%. The rate at which dew increases and evaporates under the two kinds of humidity were basically the same, but the start time of dewing was advanced with the increase of humidity, indicating that the main reason for the increase of dew quality with humidity was that the increase of humidity led to the increase of dewing time. Figure 15(b) shows the change curve of the daily maximum amount of dewing with humidity. It can be seen that the critical humidity for dewing is 51%, and then the mass of dew increases exponentially with humidity.

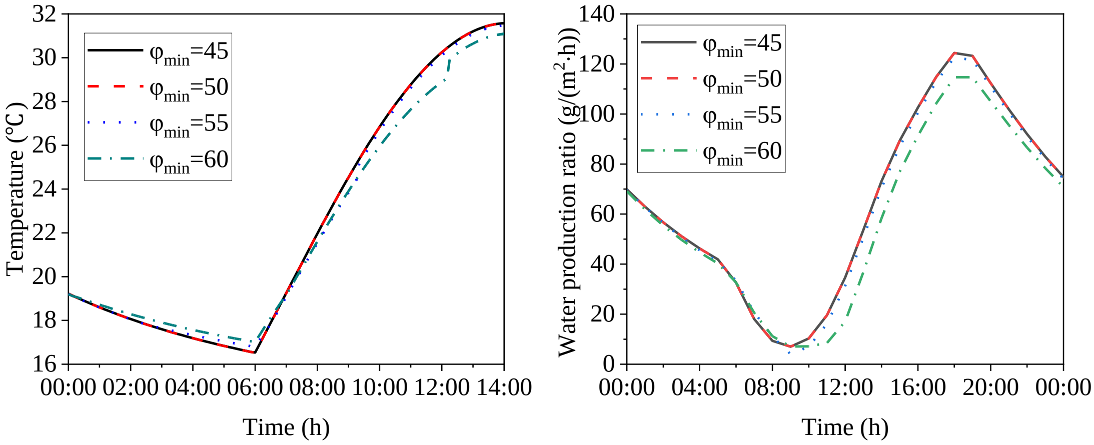

(a) Collector cover temperature

(b) water production ratio

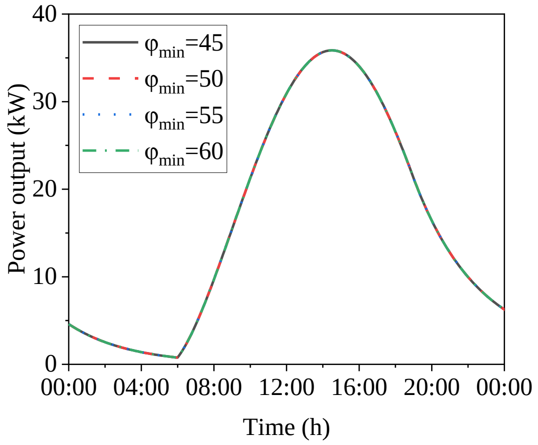

(c) Power output

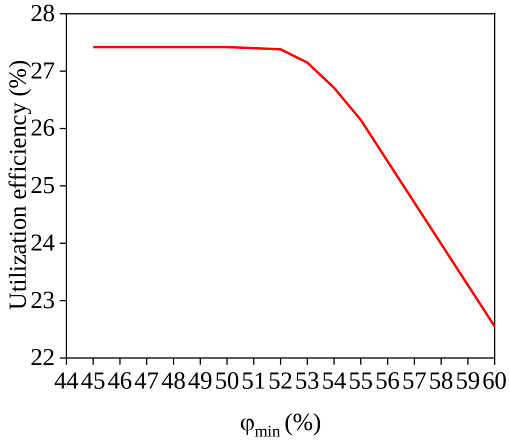

(d) Daily solar energy utilization efficiency

Figure 16. Effect of relative humidity on system performance

Figure 16 shows the influence of relative humidity on the collector cover temperature, system water production ratio, power output, and solar energy utilization efficiency. It can be seen from Figure 16(a) that during the dewing period the collector cover temperature increases with the increase of $\varphi_{\min}$, and with the increase of dewing time, the collector cover temperature increase rate gradually increased. After sunrise, there is little difference in the collector cover temperature when $\varphi_{\min}$ is 45%, 50%, and 55% respectively, but when $\varphi_{\min}$ is 60%, due to a large amount of dew, the heat absorbed by dew evaporation has a greater impact on the collector cover temperature, that is, the collector cover temperature has decreased significantly. The change in hourly water yield per unit area of the hybrid system also confirms the above analysis. After 10:00, when $\varphi_{\min}$ is 60%, due to dew evaporation the water production ratio is lower than that without dewing, which indicates that dewing in a high humidity environment does have a great negative impact on system performance. Figure 16(c) shows that the system power output under several relative humidity conditions is almost equal, indicating that dewing under high humidity conditions has little impact on the power output of SCPPSD.

The evaluation of the impact of $\varphi_{\min}$ on the daily solar energy utilization efficiency of the system can more comprehensively reflect the impact of relative humidity on dewing and system performance. The change in daily solar energy utilization efficiency under different $\varphi_{\min}$ conditions in Figure 16(d) shows that dewing caused by high humidity has a large negative impact on the daily solar energy utilization efficiency of SCPPSD. When $\varphi_{\min}$ increases from 45% to 60%, daily solar energy utilization efficiency decreases from 27.4% to 22.5%, a decrease of 4.9 percentage points.

6 Conclusion

In this paper, considering the convection heat transfer mechanism of the collector of SCPPSD, the disturbance to the hot airflow in the collector caused by the oblique-toothed flow channel boundary formed by the distillation pool cover, and the influence of dewing and dew evaporation of the collector cover, the construction of the refined mathematical model of SCPPSD unsteady heat and mass transfer is carried out, and the influence of dewing and dew evaporation of the collector cover and the oblique-toothed flow channel boundary on the system performance is discussed. The research results show that:

(1) The correlation coefficients between the calculated values of solar irradiance, ambient temperature, collector cover temperature, hot airflow temperature, distillation pool cover temperature, seawater temperature, and chimney inlet airflow temperature and the test values are all greater than 90%, and the root mean square error is less than 10%, indicating that the refined mathematical model developed in this paper can accurately reflect and evaluate the changes of SCPPSD's operating characteristics and output characteristics.

(2) It is feasible and more appropriate to use the forced convection heat transfer coefficient of the corrugated pipe to consider the influence of the oblique-toothed flow channel boundary of the distillation pool cover on the airflow disturbance. Under this scheme, the numerical calculation error of the temperature of collector cover, hot airflow, distillation pool cover, seawater, and hot airflow in the chimney is smaller, and the mathematical model taking into account the influence of the oblique-toothed flow channel boundary is more accurate for the evaluation of the operating performance of SCPPSD.

(3) The dew evaporation period and dew quality calculated by the model in this paper are close to the test results in the literature[34], which shows the reliability of the dewing model calculation in this paper. When the minimum ambient humidity $\varphi_{\min}$ is 53%, for SCPPSD, due to the effect of seawater heat storage at night, the collector cover temperature decreases at night, but the mass of dew is small, and dewing has little effect on the system performance. Dewing reduced the daily solar energy utilization efficiency of the system by 0.27 percentage points, indicating that the SCPPSD coupled with the SCPP and the disc distillation pool has a better anti-dewing negative impact characteristic.

(4) Under the meteorological conditions in this paper, the critical $\varphi_{\min}$ of dewing is 51%, and then the mass of dew increases exponentially with $\varphi_{\min}$. The high humidity leads to a surge in the mass of dew, which has a great negative impact on the water production ratio of the system. When $\varphi_{\min}$ increases from 45% to 60%, the daily solar energy utilization efficiency decreased from 27.4% to 22.5%, a decrease of 4.9 percentage points.

Acknowledgment

This research was financially supported by National Natural Science Foundation of China (No. 51976053).

Nomenclature

Symbols		η	Efficiency (-)
A	Area (m^2)	φ	Relative humidity
C_p	Specific heat capacity at constant pressure (J/kg•K)	λ	Thermal conductivity (W/m•K)
d	Characteristic length (m), Atmospheric moisture content (-)	μ	Viscosity (kg/m•s)
e	Root mean square (-)	σ	Stephan-Boltzmann constant (W/m^2•K^4)
f	Darcy friction coefficient (-)	ρ	Density (kg/m^3)
g	Gravitational constant (m/s^2)	τ	Transmittance (-)

h	Convective heat transfer coefficient ($W/m^2 \cdot K$)		
		Subscripts	
H	Height (m)	a	Ambient
l	Characteristic length (m)	b	Bottom of the distillation pool
L	Latent heat of vaporization (KJ/kg)	c	Collector cover, Convective
Le	Lewis number (-)	ch	Chimney
m_e	Water production ratio ($g/m^2 \cdot h$)	col	Collector
$\dot{m}$	Mass flow rate (kg/s)	con	Condensation
M	Weight (kg)	eva	Evaporation
p	Pressure (Pa)	ew	Evaporation of water
P_e	Output power (W)	f	Flow
$\Pr$	Prandtl number (-)	g	Glass cover of the distillation pool
q	Heat (W)	h	Height
r	Correlation coefficient (-)	in	Inlet of chimney
Re	Prandtl number (-)	kb	Heat conduction of the bottom
RH	Relative humidity (-)	r	Radiant
S	Solar radiation (W/m^2)	s	Sky
t	Time(h)	set	Sunset
T	Temperature (K)	sv	Saturated water vapor
U	Thermal resistance of heat conduction ($W/m^2 \cdot K$)	tur	Turbine
v	Velocity (m/s)	w	Water
Greek letters		*Acronyms*	
α	Roof absorption coefficient (-)	SCPP	Solar chimney power plant
Δ	Difference	SCPPSD	Solar chimney power plant integrated seawater desalination
ε	Emissivity (-)	PVDSCP	Photovoltaic and desalination based

solar chimney power plant

Reference

[1] L. Zuo, Y. Zheng, Z. Li, Y. Sha, Solar chimneys integrated with sea water desalination [J], Desalination, 276 (2011) 207-213 https://doi.org/10.1016/j.desal.2011.03.052.

[2] L. Zuo, L. Ding, J. Chen, X. Zhou, B. Xu, Z. Liu, Comprehensive study of wind supercharged solar chimney power plant combined with seawater desalination [J], Solar Energy, 166 (2018) 59-70 https://doi.org/10.1016/j.solener.2018.03.041.

[3] L. Zuo, Z. Liu, L. Ding, N. Qu, P. Dai, B. Xu, Y. Yuan, Performance analysis of a wind supercharging solar chimney power plant combined with thermal plant for power and freshwater generation [J], Energy Conversion and Management, 204 (2020) https://doi.org/10.1016/j.enconman.2019.112282.

[4] L. Zuo, N. Qu, L. Ding, P. Dai, Z. Liu, B. Xu, Y. Yuan, A vortex-type solar updraft power-desalination integrated system [J], Energy Conversion and Management, 222 (2020) https://doi.org/10.1016/j.enconman.2020.113216.

[5] L. Zuo, Z. Yan, N. Qu, P. Dai, T. Zhou, Y. Zheng, Y. Ge, Solar chimney power plant combined with membrane distillation (SCPPMD), part I: Principle and operation characteristics [J], Energy Conversion and Management, 258 (2022) https://doi.org/10.1016/j.enconman.2022.115501.

[6] S. Jo¨rg, B. Rudolf, S. Wolfgang, W. Gerhard, Design of Commercial Solar Updraft Tower Systems—Utilization of Solar Induced Convective Flows for Power Generation [J], Journal of Solar Energy Engineering, 127 (2005) https://doi.org/10.1115/1.1823493.

[7] W. Haaf, Solar Chimneys [J], International Journal of Solar Energy, 2 (2007) 141-161 https://doi.org/10.1080/01425918408909921.

[8] W. Haaf, SOLAR CHIMNEYS - PART II: PRELIMINARY TEST RESULTS FROM THE MANZANARES PILOT PLANT [J], International Journal of Solar Energy, 2 (1984) 141-161 https://doi.org/10.1080/01425918408909921.

[9] M.A. dos S. Bernardes, A. Voß, G. Weinrebe, Thermal and technical analyses of solar chimneys [J], Solar Energy, 75 (2003) 511-524 https://doi.org/10.1016/j.solener.2003.09.012.

[10] J.P. Pretorius, D.G. Kröger, Critical evaluation of solar chimney power plant performance [J], Solar Energy, 80 (2006) 535-544 https://doi.org/10.1016/j.solener.2005.04.001.

[11] M. Aurélio dos Santos Bernardes, T.W. Von Backström, D.G. Kröger, Analysis of some available heat transfer coefficients applicable to solar chimney power plant collectors [J], Solar Energy, 83 (2009) 264-275 https://doi.org/10.1016/j.solener.2008.07.019.

[12] J.-y. Li, P.-h. Guo, Y. Wang, Effects of collector radius and chimney height on power output of a solar chimney power plant with turbines [J], Renewable Energy, 47 (2012) 21-28 https://doi.org/10.1016/j.renene.2012.03.018.

[13] Y. Xu, X. Zhou, Q. Cheng, Performance of a large-scale solar updraft power plant in a moist climate [J], International Journal of Heat and Mass Transfer, 91 (2015) 619-629 https://doi.org/10.1016/j.ijheatmasstransfer.2015.07.124.

[14] D.K. Khidhir, S.A. Atrooshi, Investigation of thermal concentration effect in a modified solar chimney [J], Solar Energy, 206 (2020) 799-815 https://doi.org/10.1016/j.solener.2020.06.011.

[15] A. Bouchair, The effect of the altitude on the performance of a solar chimney [J], Energy, 249 (2022) https://doi.org/10.1016/j.energy.2022.123704.

[16] H. Dahire, S.R. Kannan, S.K. Saw, Effect of humidity on the performance of rooftop solar chimney [J], Thermal Science and Engineering Progress, 27 (2022) https://doi.org/10.1016/j.tsep.2021.101026.

[17] T. Ming, F. Meng, W. Liu, Y. Pan, R. Kiesgen de Richter, Analysis of output power smoothing method of the solar chimney power generating system [J], International Journal of Energy Research, 37 (2013) 1657-1668 https://doi.org/10.1002/er.2986.

[18] Z. Lu, Z. Yuan, S. Yujun, L. Zhenjie, L. Wenming, Unsteady State Heat Transfer of Solar Chimney Power Generation System Associated With Seawater Desalination [J], Proceedings of the CSEE, 30 (2010) 108-114 https://doi.org/10.13334/j.0258-8013.pcsee.2010.32.018.

[19] S. Kiwan, M.d. Al-Nimr, I. Salim, A hybrid solar chimney/photovoltaic thermal system for direct electric power production and water distillation [J], Sustainable Energy Technologies and Assessments, 38 (2020) https://doi.org/10.1016/j.seta.2020.100680.

[20] K. Rahbar, A. Riasi, Performance enhancement and optimization of solar chimney power plant integrated with transparent photovoltaic cells and desalination method [J], Sustainable Cities and Society, 46 (2019) https://doi.org/10.1016/j.scs.2019.101441.

[21] N. Pasumarthi, S.A. Sherif, Experimental and theoretical performance of a demonstration solar chimney model - Part I: Mathematical model development [J], International Journal of Energy Research, 22 (1998) 277-288 https://doi.org/10.1002/(SICI)1099-114X(19980310)22:3<277::AID-ER380>3.0.CO;2-R.

[22] P. Rahdan, A. Kasaeian, W.-M. Yan, Simulation and geometric optimization of a hybrid system of solar chimney and water desalination [J], Energy Conversion and Management, 243 (2021) https://doi.org/10.1016/j.enconman.2021.114291.

[23] H.Z. Hassan, Transient Analysis of a Solar Chimney Power Plant Integrated with a Solid-Sorption Cooling System for Combined Power and Chilled Water Production [J], Energies, 15 (2022) https://doi.org/10.3390/en15186793.

[24] A. Alkhalidi, Y.K. Al-Jraba'ah, Solar desalination tower, novel design, for power generation and water distillation using steam only as working fluid [J], Desalination, 500 (2021) https://doi.org/10.1016/j.desal.2020.114892.

[25] B.A. Kimball, L.A. Bellamy, Generation of diurnal solar radiation, temperature, and humidity patterns [J], Energy in Agriculture, 5 (1986) https://doi.org/10.1016/0167-5826(86)90018-5.

[26] L. Zuo, Z. Yan, P. Dai, T. Zhou, B. Qu, Y. Yuan, Y. Ge, Experimental research on the operation characteristics of solar chimney power plant combined with distillation (SCPPCD) [J], Applied Energy, 326 (2022) https://doi.org/10.1016/j.apenergy.2022.120029.

[27] X. Jinhua, STUDY OF HEAT TRANSFER ENHANCEMENT AND AXIAL LOAD-BEARING CAPABILITY OF CORRUGATED TUBES [D], Beijing University of Chemical Technology, 2006,

https://kns.cnki.net/KCMS/detail/detail.aspx?dbname=CDFD9908&filename=2007161890.nh
[28] S.K. Shukla, V.P.S. Sorayan, Thermal modeling of solar stills: an experimental validation [J], Renewable Energy, 30 (2004) https://doi.org/10.1016/j.renene.2004.03.009.
[29] V. Velmurugan, K. Srithar, Solar stills integrated with a mini solar pond — analytical simulation and experimental validation [J], Desalination, 216 (2007) 232-241 https://doi.org/10.1016/j.desal.2006.12.012.
[30] L. Zuo, Y. Yuan, Z. Li, Y. Zheng, Experimental research on solar chimneys integrated with seawater desalination under practical weather condition [J], Desalination, 298 (2012) 22-33 https://doi.org/10.1016/j.desal.2012.05.001.
[31] Z. Hongfei, H. Kaiyan, C. Ziqian, Solar Desalination Technology [C], Beijing Institute of Technology Press, Beijing, 2005,
[32] M.G. Alishaev, On condensation and precipitation of atmospheric moisture in the surface layer [J], Russian Meteorology and Hydrology, 38 (2013) 522-530 https://doi.org/10.3103/s1068373913080025.
[33] Z. Lei, M. Qinglin, S. Lifan, Analysis on Dynamic Thermal Balance Model of Landscape Water andits Numerical Simulation [J], BUILDING SCIENCE, (2007) 58-61 https://doi.org/10.13614/j.cnki.11-1962/tu.2007.10.01.
[34] H.H. Al-Kayiem, M.A. Aurybi, S.I.U. Gilani, Influence of canopy condensate film on the performance of solar chimney power plant [J], Renewable Energy, 136 (2019) 1012-1021 https://doi.org/10.1016/j.renene.2019.01.067.
[35] S. Goldstein, J.A. Naglieri, Encyclopedia of Child Behavior and Development [C], Springer, Boston, MA, https://kns.cnki.net/kcms/detail/detail.aspx?FileName=SSBDCB1800BF022462ACBDA1489BFF549CB5&DbName=GARBLAST

Appendix

Table 3. Summary of differences between this mathematical model and the original mathematical model

	This mathematical model	The original mathematical model
Heat balance equation of collector cover	$\alpha_c S(t)+q_{r,gc}=q_{r,cs}+q_{c,ca}+q_{c,cf}+q_{dew}+c_{p,c}M_c\frac{\partial T_c}{\partial t}$ Considering the influence of dewing on the system performance, the dew heat transfer term is added to the equation q_{dew}. The dewing and dew evaporation model is constructed, as shown in Section 2.3	$\alpha_c S(t)+q_{r,gc}=q_{r,cs}+q_{c,ca}+q_{c,cf}+c_{p,c}M_c\frac{\partial T_c}{\partial t}$
Convective heat transfer coefficient between the collector cover and the ambient air	When $T_c>T_a$, $h_{c,ca}=\max\left(h_1,h_2\right)$; When $T_c<T_a, h_{c,ca}=h_2$. $h_1=\frac{0.2106+0.0026v\left(\frac{\rho T_m}{\mu g\Delta T}\right)^{1/3}}{\left(\frac{\mu T_m}{g\Delta T C_p\lambda^2\rho^2}\right)^{1/3}}$ $h_2=3.87+0.0022\left(\frac{v\rho C_p}{\mathrm{Pr}^{2/3}}\right)$	$h_{\mathrm{c,ca}}=5.7+3.8v_{\mathrm{a}}$

Convective heat transfer coefficient between the collector cover and the airflow in the collector	When $T_c > T_f$, $h_{c,cf} = \max\left(h_2, h_3\right)$; When $T_c < T_f$, $h_{c,cf} = \max\left(h_1, h_2, h_3\right)$. $h_3 = \dfrac{\left(f/8\right)\left(\mathrm{Re}-1000\right)\mathrm{Pr}}{1+12.7\left(f/8\right)^{1/2}\left(\mathrm{Pr}^{2/3}-1\right)}\dfrac{\lambda}{d_h}$	$h_{c,cf} = \dfrac{\left(f/8\right)\left(\mathrm{Re}-1000\right)\mathrm{Pr}}{1+12.7\left(f/8\right)^{1/2}\left(\mathrm{Pr}^{2/3}-1\right)}\dfrac{\lambda}{d_h}$
Convective heat transfer coefficient between the distillation pool cover and the hot airflow	$h_{c,gf} = 0.02313\,\mathrm{Re}^{0.8061}\,\mathrm{Pr}^{1/3}\dfrac{\lambda}{d_h}$	$h_{c,gf} = \dfrac{\left(f/8\right)\left(\mathrm{Re}-1000\right)\mathrm{Pr}}{1+12.7\left(f/8\right)^{1/2}\left(\mathrm{Pr}^{2/3}-1\right)}\dfrac{\lambda}{d_h}$

Table 4. Comparison between the numerical results of two models and the experimental results

Physical quantity	This model *e* (%)	Original model *e* (%)	This model *r* (%)	Original model *r* (%)
Collector cover temperature	7.58	97.9	9.61	95.0
Hot airflow temperature in the middle section of the collector	6.48	94.7	9.37	95.1
Distillation pool cover temperature	1.72	99.2	3.84	98.5
Seawater temperature	2.13	99.7	4.61	99.4
Airflow temperature at chimney inlet	8.44	90.6	9.01	91.7
Hourly water yield per unit area	33.6	97.7	34.0	93.5

Note: To facilitate the comparison with the test results, the structural parameters in the two calculation models uniformly adopt the basic structural dimensions of the small SCPPSD test device shown in Figure 5. The meteorological conditions are still the climatic conditions measured on the test day of August 1, 2021